Dual nature of the math xmlns="http://www.w3.org/1998/Math/MathML">msub>mi >Be/mi>mi>Ga/mi>/msub>/math> acceptor in GaN: Evidence from photoluminescence

M. A. Reshchikov, M. Vorobiov, O. Andrieiev, D. O. Demchenko, B. McEwen, and F. Shahedipour-Sandvik

Phys. Rev. B **108**, 075202 — Published 15 August 2023

DOI: 10.1103/PhysRevB.108.075202

Dual Nature of the Be_{Ga} Acceptor in GaN: Evidence from Photoluminescence

M. A. Reshchikov, M. Vorobiov, O. Andrieiev, and D. O. Demchenko

Department of Physics, Virginia Commonwealth University, Richmond, VA 23220, USA

B. McEwen and F. Shahedipour-Sandvik

College of Nanoscale Science and Engineering, SUNY Polytechnic Institute, Albany NY 12203, USA

Abstract

Experimental studies of Be-doped GaN by photoluminescence (PL) confirmed theoretical predictions that the Be_{Ga} acceptor in GaN has dual nature, namely a coexistence of a deep state with a localized hole and a shallow state with a delocalized hole. Electron transitions via the deep polaronic states of this defect cause the broad yellow luminescence band with a maximum at 2.1-2.2 eV. Analysis of the PL dependence on temperature reveals two polaronic configurations (labeled Be1 and Be2) with the –/0 transition levels at 0.3-0.4 eV above the valence band. The Be1-related luminescence band transforms into the Be2-related luminescence band at a critical temperature of about 100 K. In addition, the shallow state of the Be_{Ga} (Be3) is found at 0.2 eV above the valence band. The associated ultraviolet PL band with the main peak at 3.26 eV can be activated by transitions of holes from state Be2 to state Be3 over a potential barrier at $T > 100$ K. The origin of another Be-related acceptor with a level at 0.113 eV above the valence band, which is responsible for the ultraviolet PL band with a maximum at 3.38 eV, remains unknown. We do not find experimental evidence for the dual nature of other acceptors, such as Mg_{Ga} in GaN and Li_{Zn} in ZnO.

I. INTRODUCTION

First-principles calculations predict the dual nature of acceptors in semiconductors [1,2]. Lany and Zunger [1] proposed in particular that the Be_{Ga} acceptor in GaN has two configurations: a deep (polaronic) state with the –/0 charge transition level at 0.45 eV above the valence band maximum (VBM) and a "shallow transient state" with a delocalized wavefunction and the –/0 level at 0.15 eV above the VBM. According to Lyons et al. [3], the polaronic state of the Be_{Ga} (hole localization on c-axis N neighbor) is at 0.55 eV above the VBM, by about 0.02 eV deeper than another polaronic state (hole localization on planar N neighbors). Cai et al. [4] calculated the deep state at 0.65 eV above the VBM. Demchenko et al. [5], using the Heyd-Scuseria-Ernzerhof (HSE) hybrid functional tuned to fulfill the generalized Koopmans condition, have found for the Be_{Ga} acceptor a deep polaronic state at 0.58 eV and a shallow effective-mass state at 0.24 eV above the VBM.

Photoluminescence (PL) is a powerful tool for analyzing point defects in semiconductors. The charge transition levels can be found with high accuracy from PL experiments when a zero-phonon line (ZPL) is observed [6]. However, due to strong electron-phonon coupling, PL bands from deep defects in GaN are usually broad and structureless. The charge transition level (or acceptor ionization energy) for such defects can be found from PL quenching dependence, yet the error in such cases may be significant.

Several attributions of Be-related PL bands in GaN (to be revised in the current work) were proposed from PL experiments. In particular, the ultraviolet luminescence (UVL_{Be}) band with a maximum at 3.38 eV, followed by a few LO phonon replicas, was ascribed to the shallow state of the Be_{Ga} acceptor with the –/0 level at 0.113 eV above the VBM [5,7,8,9,10]. The yellow band with a maximum at 2.2 eV in GaN:Be was attributed to the $Be_{Ga}O_N$ donor [11], the $Be_{Ga}V_NBe_{Ga}$

acceptor [12], and the Be_iV_{Ga} complexes [13]. The red band with a maximum at 1.8 eV was associated with the V_NBe_{Ga} complex [12].

Recently, we investigated Be-related PL from more than 100 GaN samples, including Be-doped GaN layers grown on sapphire substrates by molecular beam epitaxy (MBE) [5,12], GaN layers grown by hydride vapor phase epitaxy (HVPE) and implanted with Be [14] or co-implanted with Be and F [15], and Be-doped GaN layers on sapphire grown by metalorganic chemical vapor deposition (MOCVD) [16,17]. In almost all the samples, the dominant PL band was the broad yellow band (YL_{Be}) with a maximum at 2.15 eV. Initially, we associated it with the $Be_{Ga}V_NBe_{Ga}$ complex [12]. However, recent experimental data favored its attribution to the deep (polaronic) state of the Be_{Ga} acceptor [17]. The quantum efficiency of the YL_{Be} band approaches unity in GaN:Be samples grown by MOCVD [16,17].

In this work, we show that the YL_{Be} band consists of two unresolved bands (YL_{Be1} and YL_{Be2}) caused by electron transitions via two deep polaronic states of the Be_{Ga} acceptor (Be1 and Be2) with the levels at 0.3-0.4 eV above the VBM (throughout the paper by "energy levels" we mean acceptor binding energies or thermodynamic transition energies). In addition, a shallow state of the Be_{Ga} acceptor is found at 0.2 eV above the VBM. The properties of another Be-related acceptor, which is thought to be the shallowest acceptor in GaN (responsible for the UVL_{Be} band caused by electron transition via the level located at 0.113 eV above the VBM [5]) are beyond the scope of this paper.

II. EXPERIMENTAL DETAILS

A. Samples

Several GaN:Be samples were selected for detailed analysis (Table I).

Table I. Parameters of GaN:Be samples (SI is semi-insulating)

Sample	Growth method	Source of Be	[Be] (cm^{-3})	n (cm^{-3})
R26	MOCVD	Doping	6×10^{17}	1×10^{18}
R39	MOCVD	Doping	2×10^{19}	SI
R50	MOCVD	Memory effect	$<10^{17}$	1×10^{16}
R68	MOCVD	Doping	1×10^{18}	SI
R95	MOCVD	Doping	3×10^{18}	SI
0408a,b	MBE	Doping	5×10^{17}	SI
0020-1	MBE	Doping	7×10^{18}	5×10^{17}
Si-12-12-1100	HVPE	Implantation	5×10^{16}	1×10^{18}

Samples with prefix "R" are ~500 nm-thick GaN:Be layers grown on unintentionally doped GaN on c-plane sapphire substrates in a vertical cold wall MOCVD reactor. Beryllium acetylacetonate ($Be(acac)_2$) from Strem Chemicals was used as Be precursor. Immediately after growth, the material was annealed *in situ* under flowing N_2 at 500 Torr and 750 °C for 30 min without removing from the growth chamber. Sample R50 was contaminated with Be due to the "memory effect" after several MOCVD growths with Be source. Other details about the growth can be found elsewhere [16,17]. Sample 0020-1 is a Be-doped GaN layer grown by MBE on the c-plane sapphire substrate at West Virginia University [18]. The sample is conductive *n*-type. More details can be found in Ref. [12]. Sample Si-12-12-1100 is a Si-doped GaN layer grown on a sapphire substrate by HVPE. The sample was implanted at 600 °C with $^{9}Be^{+}$ and $^{19}F^{+}$ ions. After implantation, the

sample was annealed in N_2 ambient at T_{ann} = 1100 °C for 1 h. Other details can be found in Ref. [15].

B. Measurement Details

Steady-state PL (SSPL) was excited with a HeCd laser, dispersed by a 1200 rules/mm grating in a 0.3-m monochromator, and detected by a cooled photomultiplier tube. Time-resolved PL (TRPL) was excited with a pulsed nitrogen laser and analyzed with an oscilloscope. A closed-cycle optical cryostat was used for temperatures between 18 and 320 K. The internal quantum efficiency (IQE) for each PL band, η_i, was found by comparing the intensity after integrating over the PL band with that from calibrated GaN samples [6,19,20]. The as-measured PL spectra were corrected for the measurement system's spectral response. The PL intensity was additionally multiplied by λ^3, where λ is the light wavelength, to present the PL spectra in units proportional to the number of emitted photons as a function of photon energy [6,21]. Other details of PL experiments can be found elsewhere [6,21]

III. RESULTS

A. Two-step quenching of the YL_{Be} band

Low-temperature PL spectra for two representative samples are shown in Fig. 1. The near-band-edge (NBE) band consists of the donor-bound exciton (DBE) and free exciton (FE) peaks that can be distinguished with increasing temperature. The UVL_{Mg} band with the main peak at 3.27 eV followed by LO phonon replicas is attributed to the shallow Mg_{Ga} acceptor unintentionally introduced during MOCVD growth. The broad YL_{Be} band with a maximum at 2.15 eV is attributed to the Be_{Ga} acceptor and will be analyzed below.

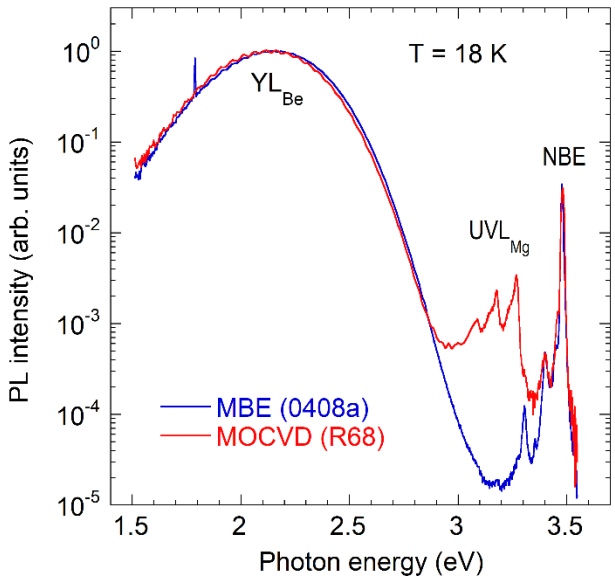

Fig. 1. Normalized PL spectra from MBE and MOCVD GaN:Be samples at T = 18 K. The NBE band consists of unresolved DBE and FE peaks at about 3.48 eV and two LO phonon replicas of the FE peak. The UVL_{Mg} band with the main peak at 3.27 eV is caused by contamination with Mg during MOCVD growth. The broad YL_{Be} band with a maximum at 2.15 eV is attributed to the polaronic state of the Be_{Ga} acceptor.

In all Be-doped GaN samples, the YL_{Be} band is quenched by the two-step mechanism [17]. In the first step, at $T_1 \approx 100$ K, the YL_{Be} intensity decreases by R_1. For the majority of GaN:Be samples, R_1 = 1.3–2. However, for a few samples grown by MBE, the magnitude of the first step is larger, up to R_1 = 10. After the first step, a plateau is usually observed in the temperature dependence before the second quenching begins at $T_2 \approx 200$ K. For conductive n-type GaN:Be samples, the activation energy E_A = 0.30 eV and hole-capture coefficient $C_p \approx 4\times10^{-7}$ cm^3/s were found from the second quenching [12]. Sometimes, the slope in the Arrhenius plot is smaller, yet still, it can be concluded that $E_A \approx 0.30$ eV [17]. In semi-insulating (SI) GaN:Be samples, both steps are tunable by excitation intensity, and the second quenching occurs by the abrupt and tunable quenching mechanism [20]. From the analysis of the $T_1(G)$ and $T_2(G)$ dependences in SI samples,

where G is the electron-hole generation rate, we concluded that these steps correspond to activation energies of about 0.15 and 0.3 eV, respectively [12,17].

The second step at $T_2 \approx 200$ K was previously explained by the thermal emission of holes from the Be_{Ga} state at 0.30 eV to the valence band [17]. The main proof for this quenching mechanism (the Schön-Klasens mechanism) is the concurrent increase in the NBE emission intensity [6,19]. The rise of PL intensity by up to a factor of 10 in some GaN:Be samples indicates that the IQE of the YL_{Be} band just below T_2 is about 0.9 in these samples [17].

However, the first step cannot be explained by the thermal emission of holes to the valence band [17]. In particular, in samples with the IQE close to unity, the first step of the YL_{Be} quenching does not cause any changes in the intensities of other PL bands. Below, we present experimental evidence indicating that the first step corresponds to replacing the broad yellow band with a very similar one, redshifted by 40-50 meV. Hereafter, we will call these components of the YL_{Be} band the YL_{Be1} and YL_{Be2}.

1. Abrupt red shift of the YL_{Be} band

Figure 2 shows the temperature dependences of the YL_{Be} band's position of the maximum, $\hbar\omega_{max}$, and PL intensity, I^{PL}. Concurrently with the first quenching step between 70 and 100 K, the band maximum red-shifts by $\Delta\hbar\omega_{max} \approx 40$ meV [Fig. 2(a)]. In SI samples, where the quenching is tunable by excitation power density, P_{exc}, the shifts coincide with the first quenching step [Fig. 2(b)]. The abrupt red shift of the YL_{Be} band's maximum concurrently with the first quenching step was confirmed in more than ten GaN:Be samples, including conductive *n*-type and SI samples grown by MOCVD and MBE. In other samples, the position of the YL_{Be} band could not be reliably analyzed, mainly because of severe Fabry-Perot interference modulating the spectrum.

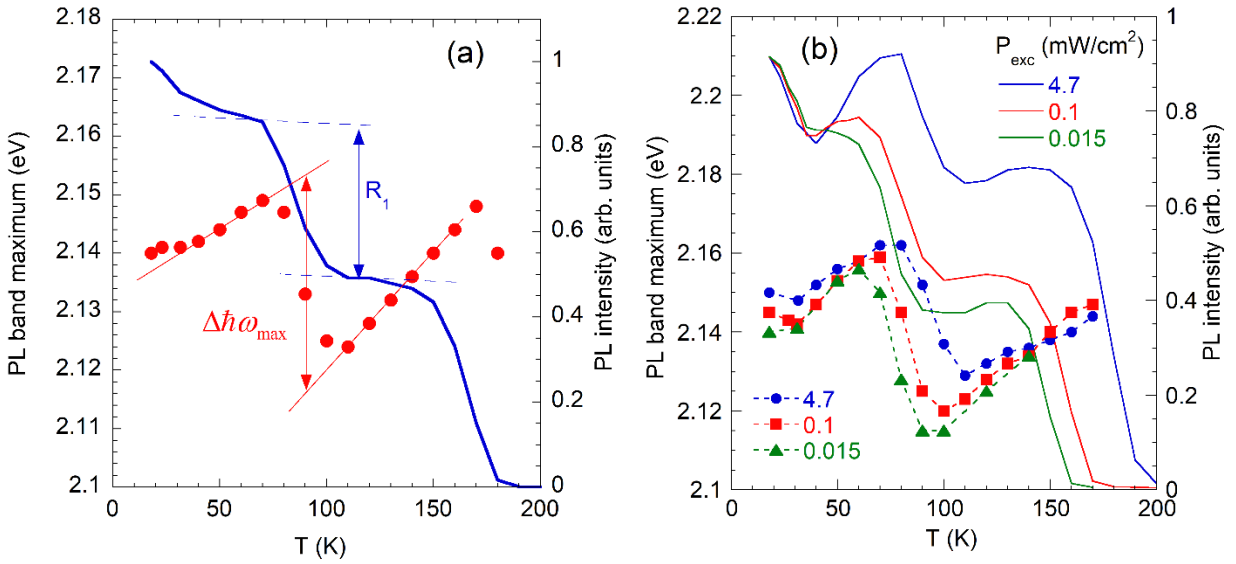

Fig. 2. Temperature dependences of $\hbar\omega_{max}$ (symbols) and I^{PL} (solid lines) for the YL_{Be} band in GaN:Be grown by MOCVD. (a) sample R95, P_{exc} = 0.002 W/cm^2. (b) sample R50, P_{exc} = 1.5×10^{-5}, 10^{-4}, and 0.0047 W/cm^2. At $T \approx$ 80-100 K, the YL_{Be} intensity drops by $R_1 \approx 2$, and the YL_{Be} band red-shifts by $\Delta\hbar\omega_{max}$ = 40-50 meV.

2. Temperature dependence of the YL_{Be} lifetime

For electron transitions from the conduction band to a defect level in conductive *n*-type GaN, the temperature dependence of PL intensity, IQE ($\eta = I^{PL}/G$), and PL lifetime (τ) can be fitted with the following expression [22,23]

$$\frac{I^{PL}(T)}{I^{PL}(0)} = \frac{\eta(T)}{\eta_0} = \frac{\tau(T)}{\tau_0} = \frac{1}{1+(1-\eta_0)\tau_0 C_p N_v g^{-1}\exp(-E_A/kT)}. \quad (1)$$

Here, η_0, $I^{PL}(0)$, and τ_0 are the IQE, PL intensity, and PL lifetime at temperatures before quenching, C_p is the hole-capture coefficient, g is the degeneracy of the defect level (assumed to be 2), N_v is the effective density of states in the valence band ($N_v = 3.2\times10^{15}T^{3/2}$ cm^{-3}), k is Boltzmann's constant, and E_A is the activation energy (the energy distance from the defect level to the valence band plus a barrier for the hole capture if any). The parameter τ_0 can be found in TRPL

measurements. When the PL decay is not purely exponential (e.g., when the contribution of donor-acceptor-pair transitions is significant at low temperature), τ_0 can be defined as the time at which the $I^{PL}(t)t$ dependence has a maximum [24]. τ_0 depends on the concentration of free electrons (n) in conductive n-type GaN as

$$\tau_0 = \frac{1}{nC_n}, \quad (2)$$

where C_n is the electron-capture coefficient.

The YL_{Be} lifetime is inversely proportional to the n, with $C_n = 1\times10^{-13}$ cm^3/s [15,17]. This observation indicates that the YL_{Be} band is caused by electron transitions from the conduction band to the deep defect level. The $\tau(T)$ dependence for the YL_{Be} band in one of the samples is shown in Fig. 3(a). This initially Si-doped HVPE GaN sample was implanted with Be and F and then annealed at T = 1100 °C [15]. The sample behaves as a degenerate n-type GaN with $n \approx 10^{18}$ cm^{-3}. The YL_{Be} lifetime does not change between 18 and 100 K ($\tau_0 \approx 11$ μs). However, concurrently with the first quenching step, τ decreases to 3 μs. The $I^{PL}(t)t$ dependence broadens near $T = T_1$, and the effective lifetime returns to a higher value ($\tau_0 \approx 9$ μs) between 135 and 180 K. At $T > T_1$, the $\tau(T)$ dependence is identical to the $I^{PL}(T)$ dependence and can be fitted with Eq. (1) with typical parameters for the YL_{Be} band. The discontinuity of the YL_{Be} lifetime concurrently with the first quenching step was confirmed in all GaN:Be samples where temperature dependence of TRPL was carefully studied.

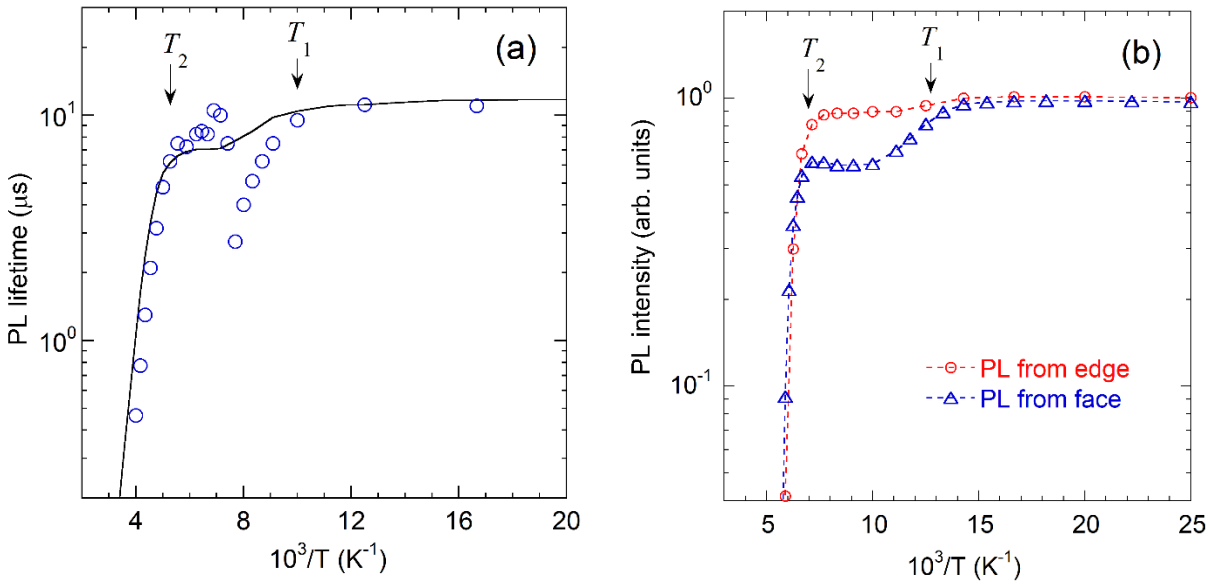

Fig. 3. (a) Temperature dependence of the YL_{Be} lifetime (circles) and PL intensity (solid line) in *n*-type HVPE GaN implanted with Be and F and annealed at 1100 °C (sample Si-12-12-1100). (b) Temperature dependence of the YL_{Be} intensity (normalized at 18 K) for MOCVD-grown GaN sample R68 measured in two geometries. P_{exc} = 5×10^{-5} W/cm^2.

3. The origin of the first quenching step

From the analysis of the temperature dependences of the YL_{Be} band position and PL lifetime, we conclude that the broad YL_{Be} band consists of two unresolved components: YL_{Be1} and YL_{Be2}. The YL_{Be1} band has a slightly longer PL lifetime and dominates at $T < T_1$. It is caused by electron transitions from the conduction band (or from shallow donors in nondegenerate samples at $T < 50$ K) to state Be1 with the characteristic time τ_1. At $T > T_1$, the YL_{Be1} band vanishes and is replaced with the YL_{Be2} band. The latter has a maximum at lower photon energies (by about 0.05 eV) and is caused by electron transitions from the conduction band to state Be2 with PL lifetime τ_2. The drop of PL intensity by R_1 in the first step is explained below.

Suppose the hole-capture mechanism does not change during the first quenching step. In that case, the IQE of recombination via the Be_{Ga} defect should not change, which raises the question of why PL intensity decreases. We assume that the IQE of the YL_{Be} band *inside* the sample does not change at $T = T_1$, while different light extraction efficiencies of PL from the YL_{Be1} and YL_{Be2} bands cause the step in the *measured* PL signal. In other words, optical dipoles parallel to the c-axis of the crystal are expected to have lower extraction efficiency for PL observed from the sample's c-plane. To test this assumption, we measured the temperature dependence of the YL_{Be} intensity after turning the sample by 90 degrees and collecting PL from the cleaved edge of the sample. The $I^{PL}(T)$ dependence from the sample edge is shown in Fig. 3(b) in comparison with that obtained from the sample's face in the usual geometry. The R_1 decreased from 1.7 to 1.1, whereas other features of the YL_{Be} band, including the shape, position, and the red-shift of the PL band during the first step, remained unchanged.

The step can also be formally explained by the assumption that the transition via state Be1 is purely radiative while that via state Be2 is partly nonradiative (or reduced extraction efficiency), with the nonradiative fraction $\gamma = 1 - R_1^{-1}$. Before describing the model of the Be_{Ga} acceptor in more detail, we will resolve an exciting puzzle about the UVL band in Be-doped GaN.

B. New UVL band

1. Emerging with temperature UVL band

The second unique feature observed in most GaN:Be samples is the emergence of the UVL band after the first quenching step is completed, but the second one has yet to begin. It is well known that the UVL band in *undoped* GaN, with the first peak at about 3.27 eV followed by weaker LO phonon replicas (labeled UVL_{Mg}, hereafter), is caused by transitions from the conduction band (or from shallow donors at $T < 50$ K) to the Mg_{Ga} acceptor, the –/0 level of which

is located at 0.223 eV above the VBM [6]. In conductive *n*-type GaN, the UVL_{Mg} band is quenched in agreement with Eq. (1). For the Mg_{Ga} acceptor, $C_p = 1\times10^{-6}$ cm^3/s and $C_n = 3.2\times10^{-12}$ cm^3/s [25,26].

The quenching of the UVL_{Mg} band in *n*-type GaN begins at $T \approx 120$ K, with the slope in the Arrhenius plot corresponding to $E_A \approx$160-180 meV [6]. However, in Be-doped GaN samples, the UVL band intensity *increases*(!) exponentially with a temperature above 120 K. An example is shown in Fig. 4 for a conductive *n*-type GaN:Be sample grown by MBE [12]. At temperatures between 18 and 110 K, the UVL_{Mg} band cannot be found in that sample. The feature at about 3.3 eV at 110 K in Fig. 4 is likely the second LO phonon replica of the NBE peak. The intensity of the UVL band increases with temperature by nearly two orders of magnitude instead of quenching between 110 and 200 K. The shape and position of this UVL band are similar to those of the UVL_{Mg} band in Mg-doped GaN [25,27].

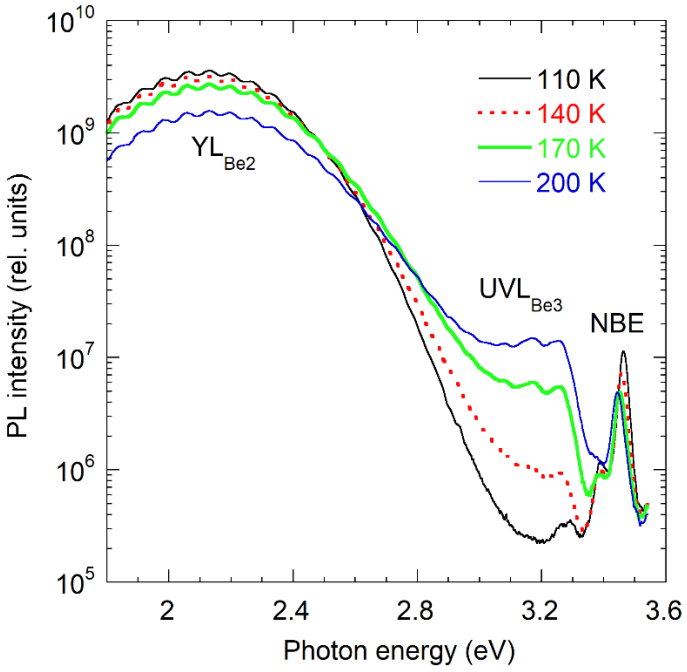

Fig. 4. SSPL spectra from MBE-grown *n*-type GaN:Be (sample 0020-1) at selected temperatures.

The emergence of the UVL band at $T > 140$ K was observed in all GaN:Be samples (about 50 samples) except for samples with relatively weak YL_{Be} band and strong background signal (e.g., from the NBE or UVL_{Mg} bands) in the blue-UV spectral region. Another example can be found in Ref. [17], where a conductive *n*-type GaN:Be sample was grown by MOCVD (sample R26). In that case, the UVL_{Mg} band was clearly observed at low temperatures (most of our MOCVD-grown GaN:Be samples were contaminated with Mg, in contrast to MBE-grown GaN:Be samples studied earlier [12]). Figure 5 shows Arrhenius plots for the integrated PL intensities (or quantum efficiencies) of three PL bands in that sample (the relative intensities of these PL bands in Figure 3 of Ref. [17] are slightly different because peak intensities were plotted there). In the fits, parameters include index i (i = 1, 2, and 3 for the YL_{Be}, UVL_{Mg}, and NBE bands, respectively).

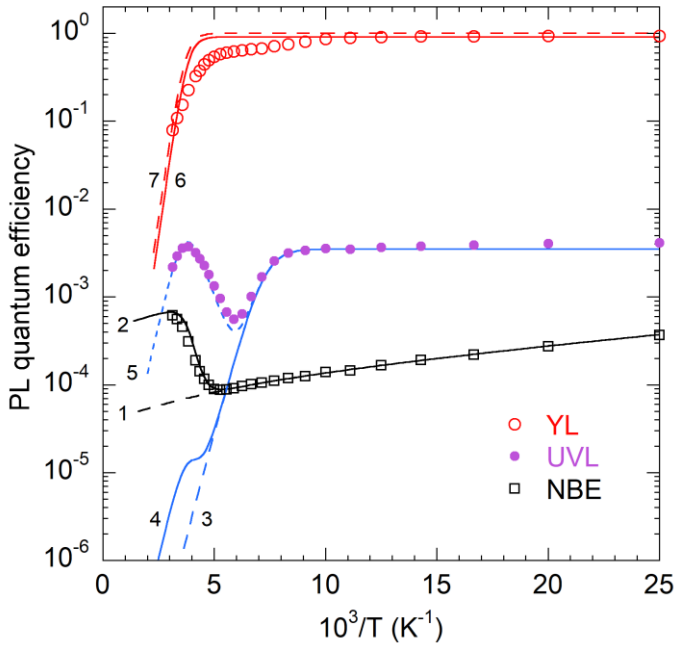

Fig. 5. Temperature dependences of PL quantum efficiencies of the YL_{Be}, UVL, and NBE bands in MOCVD-grown GaN:Be (sample R26). The symbols are experimental data, and the lines are calculated. Lines 3,6, and 7 are calculated using Eq. (1) with $\eta_{01}(0) = 0.91$, $C_{p1} = 1\times10^{-7}$ cm^3/s (line 5); $\eta_{01}(0) = 0.9998$, $C_{p1} = 3\times10^{-5}$ cm^3/s (line 6); $\tau_{01} = 10$ μs and $E_{A1} = 300$ meV for both lines; $\eta_{02}(0) = 3.5\times10^{-3}$, $C_{p2} = 1\times10^{-6}$ cm^3/s, $\tau_{02} = 0.3$ μs, $E_{A2} = 160$ meV (line

3). Line 1 is calculated with Eq. (4) with $\eta_{03}(0) = 1.5\times10^{-3}$, $C' = C'' = 20$, $E' = 6.5$ meV, $E'' = 30$ meV. Lines 2,4, and 5 account for the quenching of channel 1 according to Eq. (3) with $\eta_{01}(0) = 0.91$ (lines 2 and 4) and $\eta_{01}(0) = 0.9998$ (line 5).

2. "Negative" thermal quenching of the NBE and UVL bands

At T > 110-120 K, the UVL_{Mg} quenching begins in agreement with Eq. (1) (line 3 in Fig. 5). However, at T > 180 K, the UVL band intensity increases, and it remains relatively strong up to room temperature. The NBE intensity also increases by order of magnitude between 200 and 300 K. In [17], we explained this increase (often called "negative thermal quenching") by a competition between recombination channels for holes in the valence band. However, quantitative analysis of the data shown in Fig. 5 reveals contradictions with that explanation. Indeed, the quenching of a strong PL band (with the quantum efficiency η_1) in conductive *n*-type GaN must increase *all* PL bands (with quantum efficiencies η_i, i > 1) by $R \approx (1-\eta_{01})^{-1}$, where i labels a particular PL band and η_{01} is the IQE of the strong PL band before its quenching [19]. For example, the quenching of the Zn-related BL1 band with $\eta_{01} \approx 0.8$-0.9 resulted in a concurrent step-wise rise of the YL1 and NBE intensities by order of magnitude [6,19]. When η_{0i} changes with temperature (i.e., due to its quenching), the simplified approach may not be accurate, and the value of η_{01} can be found from the following expression, in which all parameters may depend on temperature: [19]

$$\frac{I_i^{PL}}{I_{0i}^{PL}} = \frac{\eta_i}{\eta_{0i}} = \frac{1-\eta_1}{1-\eta_{01}}. \qquad (3)$$

Here, I_i^{PL} (I_{0i}^{PL}) is the integrated PL intensity of channel i with (without) account for the quenching of channel 1, and $\eta_1 = (I_1^{PL}/I_{01}^{PL})\eta_{01}$.

The $\eta_{0i}(T)$ dependence for the NBE band up to 200 K in Fig. 5 is fitted with the following empiric expression (the dashed line 1)

$$\eta_{i0} = \frac{\eta_{i0}(0)}{1 + C' \exp\left(-E'/kT\right) + C'' \exp\left(-E''/kT\right)}, \quad (4)$$

where C' and C'' are dimensionless parameters and E' and E'' are activation energies corresponding to the dissociation of bound and free excitons, respectively. By fitting the whole temperature dependence of the NBE band with Eqs. (3) and (4) (the solid line 2), we find η_{01} = 0.91 for the YL_{Be} band before its quenching. However, using this η_{01}, we obtain significant disagreement (line 4) with the experimental UVL band dependence. To achieve a formal agreement (line 5), unreasonably high values of η_{01} (0.9998) and C_p (10^{-5} cm^3/s) are needed. Note that in these fits, the $\eta_1(T)$ dependences (lines 6 and 7) were simulated to reach an agreement with the UVL and NBE data with Eq. (3), where η_{01} is the only fitting parameter. These simulated $\eta_1(T)$ dependences do not fit well the experimental dependence for the YL_{Be} band, an issue to be discussed later. We conclude that the UVL band increasing with temperature is not the Mg-related UVL_{Mg} band, despite their apparent similarities. We propose that this UVL band (labeled UVL_{Be3}, hereafter) is caused by electron transitions from the conduction band to the shallow state of the Be_{Ga} acceptor located at about 0.2 eV above the VBM.

3. Shapes and positions of the Be_{Ga}- and Mg_{Ga}-related UVL bands

The assumption that the UVL bands in GaN:Be and GaN:Mg samples are caused by different defects is supported by careful analysis of PL spectra. Figure 6(a) compares the PL spectrum near the UVL band from two GaN:Be samples at T = 190 K with that from n-type GaN:Mg sample grown by HVPE and lightly doped with Mg ([Mg] = 10^{17} cm^{-3}). The DBE peak is at 3.471 eV at T = 18 K and 3.446 eV at T = 190 K. The ZPLs at 3.270 eV (GaN:Mg) and 3.260 eV (GaN:Be) are attributed to transitions from the conduction band to the Mg and Be acceptor levels at T = 190 K. Up to two LO phonon replicas can also be resolved. The GaN bandgap is 3.48 eV at this

temperature [28]. We conclude that the acceptor level is located at 0.21 eV in GaN:Mg and 0.22 eV in GaN:Be at T = 190 K.

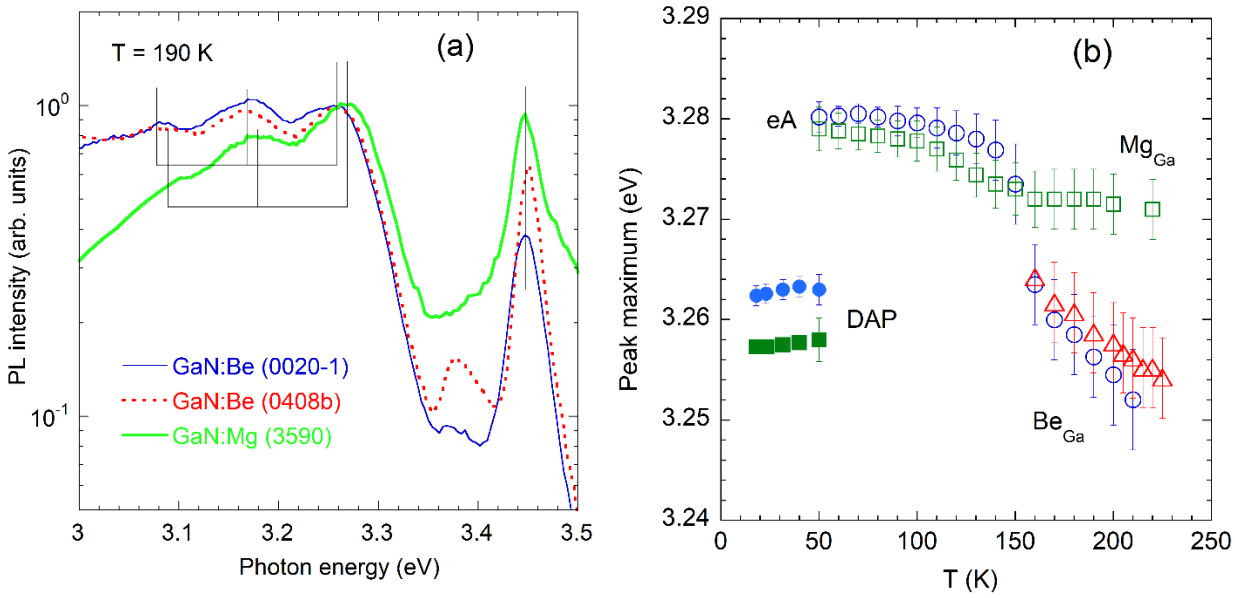

Fig. 6. (a) High-energy part of the PL spectrum from MBE GaN:Be (samples 0020-1 and 0408b) at T = 190 K in comparison with the spectrum from Mg-doped GaN grown by HVPE (sample 3590). The DBE peak is at 3.446 eV. The ZPL of the UVL band is at 3.270 eV (GaN:Mg) and 3.260 eV (GaN:Be). Two phonon replicas at distances of 90 meV are shown. (b) Dependence of PL peak positions on temperature for MOCVD GaN:Be (blue circles, sample R68), MBE GaN:Be (red triangles, sample 0408b), and HVPE GaN:Mg (green squares, sample 3590). The data for samples R68 and 0408b are shifted to lower energies by 7 meV to account for the corresponding shift in the excitonic lines due to strain in the GaN layers grown on sapphire substrates. The solid symbols show DAP peaks, and the empty symbols show the eA peaks. At T > 150 K, the UVL_{Mg} band disappears, and the UVL_{Be3} band emerges in the MOCVD GaN:Be sample. There is no UVL_{Mg} band in sample 0408b.

In samples where the Mg-related UVL_{Mg} band was observed at T < 150 K (such as sample R26 in Fig. 5), the UVL maximum abruptly red-shifted by 0.01-0.02 eV after the UVL_{Be3} intensity began increasing with temperature. Figure 6(b) shows the shifts of the UVL band with temperature in the Be-doped GaN sample grown by MOCVD (sample R68) in comparison with the data for

the Mg-doped freestanding GaN template grown by HVPE (sample 3590). In both samples, at T < 50 K, the UVL_{Mg} band is caused by electron transitions from shallow donors to the Mg_{Ga} acceptor, the so-called donor-acceptor pair (DAP) transitions [25]. At higher temperatures, transitions from the conduction band to the same acceptor (the eA transitions shown with empty symbols) cause the UVL_{Mg} band. In both samples, the quenching of the UVL_{Mg} band begins at T = 110 K. The UVL_{Mg} band in the GaN:Mg sample gradually red-shifts with increasing temperature from 50 to 220 K, totally by less than 10 meV. Note that the bandgap shrinks by 30 meV in this temperature range [28]. The eA peak of the UVL band in the GaN:Be sample red-shifts abruptly (by 10-15 meV) at $T \approx 150$ K. At the same temperature, the emergence of the UVL_{Be3} band begins. At T > 200 K, the UVL_{Be3} band abruptly quenches, together with the YL_{Be} band. The quenching is tunable by excitation intensity. This abrupt shift of the UVL band before its intensity started increasing was observed in several GaN:Be samples.

C. Time-resolved PL

Analysis of TRPL provides additional evidence that the UVL_{Be3} band is unrelated to Mg. In conductive *n*-type GaN:Be samples, the PL lifetimes of the YL_{Be} and UVL_{Mg} bands are related as 30:1 in agreement with their electron-capture coefficients ($C_n = 1\times10^{-13}$ and 3.2×10^{-12} cm^3/s, for these PL bands, respectively) [26]. However, the emerging at T > 140 K UVL band decays after a laser pulse, similarly to the YL_{Be} band [Fig. 7(a)]. The temperature dependences of PL lifetimes for these PL bands are shown in Fig. 7(b). At $T < T_1 \approx 100$ K, the PL lifetime of the YL_{Be} band is about 60 μs. Concurrently with the first quenching step, the PL lifetime decreases to 30 μs and then shows a plateau at 40-45 μs up to $T_2 \approx 180$ K. The $I^{PL}(T)$ and $\tau(T)$ dependences for the YL_{Be2} band at $T > T_2$ are identical, in agreement with Eq. (1). Surprisingly, not only the magnitude but

also the temperature dependence of PL lifetime for the UVL_{Be3} band at 3.25 eV are nearly identical to those of the YL_{Be} band at 2.2 eV.

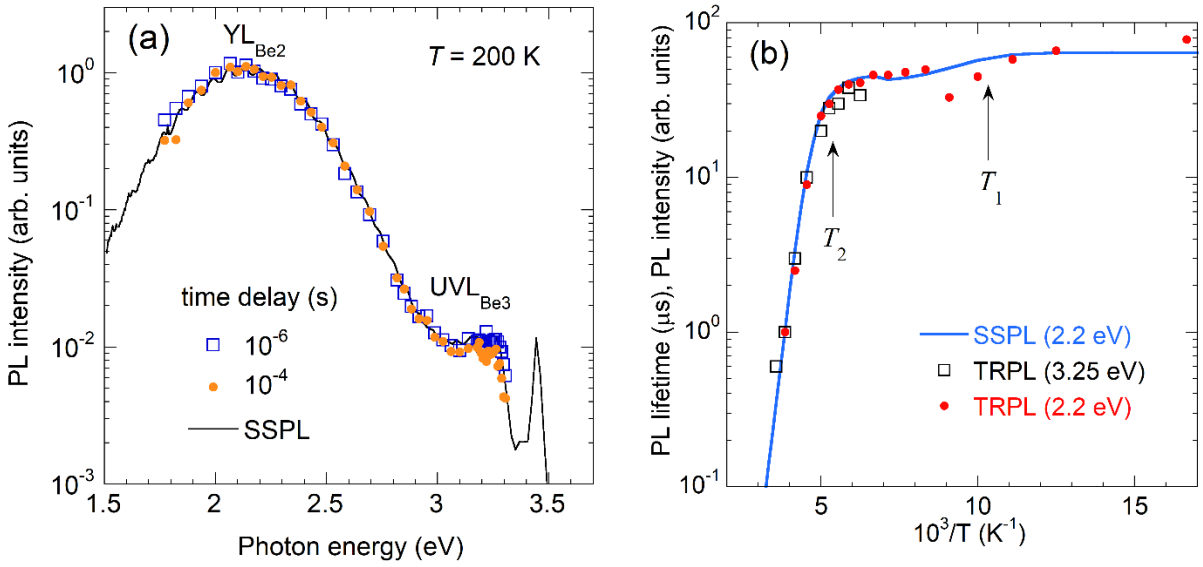

Fig. 7. TRPL results for MBE GaN:Be (sample 0020-1) (a) Normalized SSPL and TRPL spectra at T = 18 K. The TRPL spectra at 10^{-6} and 10^{-4} s after a laser pulse are nearly identical, indicating that the YL_{Be} and UVL_{Be3} bands decay with about the same characteristic time. (b) Temperature dependences of the YL_{Be} (at 2.2 eV) and UVL_{Be3} (at 3.25 eV) lifetimes in comparison with the YL_{Be} SSPL intensity.

The temperature dependences of the YL_{Be} and UVL_{Mg} lifetimes for sample R26 are shown in Fig. 8. The YL_{Be} lifetime is 11 μs at T < 100 K, begins decreasing at $T_1 \approx 110$ K, and returns to the 10 μs plateau at $T \approx 140$ K. The PL lifetime of the UVL_{Mg} band is 0.3 μs at T < 120 K, in agreement with Eq. (2) for the sample with $n = 1\times10^{18}$ cm^{-3}. The quenching of the UVL_{Mg} band at T > 130 K and simultaneous decrease of its PL lifetime with the same activation energy is explained by the thermal emission of holes from the Mg_{Ga} level to the valence band, in agreement with Eq. (1). The UVL_{Be3} band appears at higher temperatures. This band's PL lifetime magnitude and temperature dependence are *identical* to those of the YL_{Be} band.

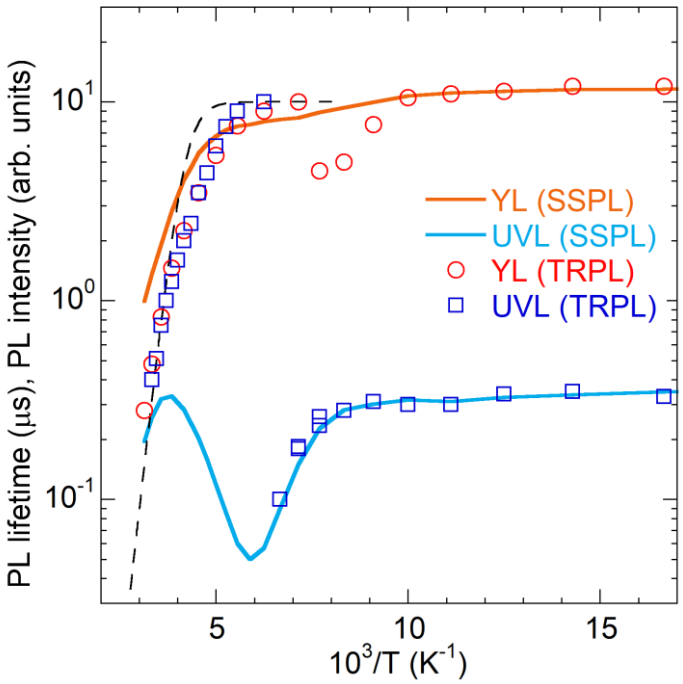

Fig. 8. Temperature dependences of the YL_{Be} (at 2.2 eV) and UVL_{Be3} (at 3.25 eV) lifetimes (symbols) in comparison with the SSPL intensity dependences (solid lines) in MOCVD-grown *n*-type GaN:Be (sample R26). The SSPL curves are shifted vertically to match the TRPL data. The dashed line is calculated using Eq. (1) with typical parameters for the YL_{Be} band (E_A = 0.30 eV).

D. Summary of the experimental results

The experimental results from a large set of Be-doped GaN samples indicate that one defect (isolated Be_{Ga} acceptor) is responsible for three PL bands. Two of these bands are very broad and contribute to the yellow part of the spectrum. The YL_{Be1} band with a maximum at 2.15 eV is observed at T < 100 K. At higher temperatures, the YL_{Be2} band replaces the YL_{Be1} band. This transition causes a step-wise decrease of the YL_{Be} intensity, an abrupt red shift of the PL band by up to 0.05 eV, and a discontinuity in the temperature dependence of the YL_{Be} lifetime. The third PL band is the UVL_{Be3} band with the main peak at 3.26 eV. The UVL_{Be3} band appears at T > 100

K, and its intensity increases exponentially with temperature. In a wide temperature range, the intensities of the YL_{Be2} and UVL_{Be3} bands *correlate*.

The ratio of the integrated intensities UVL_{Be3}/YL_{Be} for several GaN:Be samples is shown in Fig. 9. The ratio increases with temperature as $\exp(-\Delta E/kT)$ with $\Delta E = 0.14$ eV. Note that the slope of the dependence does not change after the YL quenching begins (the characteristic temperature T_2 is indicated for sample 0020-1). The same dependence is observed in all Be-doped GaN samples, grown by MOCVD and MBE, including conductive *n*-type and semi-insulating samples (in about 50 samples except for a few samples where the YL_{Be} band was too weak or a strong background signal obstructed the UVL_{Be3} band). In SI samples, the YL_{Be} band is quenched by the abrupt and tunable quenching mechanism, and both the YL_{Be} and UVL_{Be3} intensities abruptly drop at $T \approx T_2$.

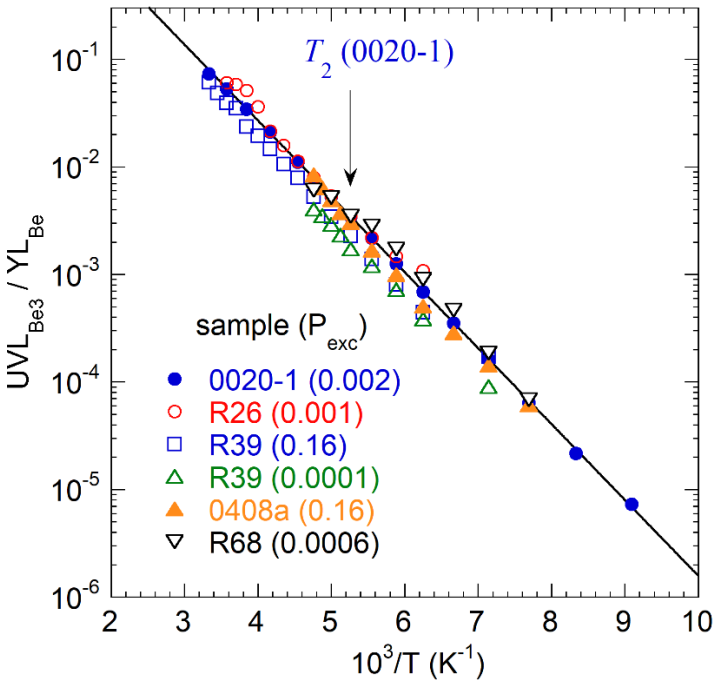

Fig. 9. Temperature dependence of the ratio of the integrated UVL_{Be3} and YL_{Be} bands in selected GaN:Be samples. P_{exc} (in W/cm^2) is given in brackets. The solid line is a fit for sample 0020-1 using Eq. (17) with the following parameters: $\Delta E_{23} = 140$ meV, $\delta = 18$.

Below, the most important experimental findings are summarized.

1. The UVL_{Be3} band is caused by electron transitions via a shallow acceptor level at E_3 = 0.21 eV above the VBM at T = 190 K. In the limit of low temperatures, this level is expected at 0.23-0.24 eV, about 10-15 meV deeper than the –/0 level of the Mg_{Ga} acceptor. The UVL_{Be3} band cannot be found at T < 100 K.
2. The YL_{Be2} and UVL_{Be3} intensities correlate in a wide range of temperatures (Fig. 9), irrespective of the temperature dependence of the YL_{Be} band (the characteristic temperatures and the effective activation energies of the YL_{Be} quenching in different samples vary significantly). The emergence of the UVL_{Be3} band at T > 100 K and the exponential ratio of the UVL_{Be3}/YL_{Be2} intensities are explained by the temperature-activated transition of the bound hole from deep state Be2 to shallow state Be3. The exponential dependence of the PL intensities ratio with the activation energy 0.14 eV indicates that the Be2 state is located 0.14 eV deeper than the Be3 state, or at E_2 = 0.38 eV above the VBM (in the limit of low temperatures).
3. The Be2 state of the Be_{Ga} acceptor is slightly deeper than the Be1 state. This follows from the fact that with increasing temperature the YL_{Be1} band is replaced with the YL_{Be2} band, and the transition is thermally activated above a potential barrier. Since the YL_{Be} maximum red-shifts by about 0.05 eV and the shape of the yellow band does not change upon the transition from Be1 to Be2 at $T \approx T_1$, we assume that the shift in the band ZPL is also about 0.05 eV; i.e., E_1 = 0.33 eV above the VBM.
4. It appears that in the whole temperature range, photogenerated holes are captured by only one of the three Be_{Ga} states, and this state feeds two others. Indeed, the intensities of other PL bands (NBE and UVL_{Mg}) do not show any deviation from their expected temperature dependences in samples where the IQE of the YL_{Be2} band is close to unity at $T_1 < T < T_2$.

5. The most likely scenario is that the shallow, effective-mass level Be3 captures holes from the valence band. The captured hole almost immediately transits to the Be1 level at low temperatures. The transition to the Be2 level is obstructed by a potential barrier. The Be2 level is the deepest of the three states. It becomes populated with holes at $T > T_1$ when holes overcome a potential barrier (either between Be3 and Be2 or between Be1 and Be2), and the defect relaxes to the lowest minimum.

6. At $T > T_2$, the thermal emission of holes from the Be_{Ga} acceptor (from the Be3 level, as will be shown below) becomes significant. Since the deeper state Be2 feeds the Be3 level with holes at these temperatures, the quenching of the UVL_{Be3} and YL_{Be2} bands is shifted to higher temperatures from the expected quenching for a shallow acceptor with the ionization energy of 0.2 eV.

7. The measured PL lifetimes for the UVL_{Be3} and YL_{Be2} bands are identical, which seems surprising at first glance. However, one should look at what is actually measured in TRPL experiments. Let's assume that the real UVL_{Be3} lifetime is much shorter than that of the YL_{Be2} band. After a laser pulse at $T > T_1$, a photogenerated hole is captured by the Be3 level and quickly transits to the Be2 level. The population of these two levels corresponds to the temperature and the energy difference between the two potential minima. Even if the hole in state Be3 quickly recombines with a free electron (with the characteristic time $\tau_{n3} = (nC_{p3})^{-1}$) in one Be_{Ga} acceptor, it will stay longer in state Be2 of another Be_{Ga} acceptor and eventually may transit to the Be3 level and produce the UVL_{Be3} band at longer delay times. In other words, the Be2 level holds the majority of holes after the laser pulse and feeds the Be3 level during the YL_{Be2} lifetime.

The experimental data with many constraints can be explained in the model suggested below.

IV. MODEL

Based on extensive experimental findings, we propose that the neutral Be_{Ga} acceptor has three states in the gap: deep states Be1 and Be2, and a shallow state Be3 [Fig. 10(a)]. HSE calculations suggest that the deep states correspond to the localization of the bound hole at the nearest N atom in the 0001 direction of the wurtzite lattice and in one of the three remaining equivalent in-plane directions. From the experiment, the –/0 transition levels of the Be1, Be2, and Be3 states are located at E_1 = 0.30 eV, E_2 = 0.34 eV, and E_3 = 0.20 eV above the VBM (at $T \approx 200$ K). Accordingly, the separations between the potential minima are $\Delta E_{21} = E_{21} - E_{12}$ = 0.04 eV, $\Delta E_{23} = E_{23} - E_{32}$ = 0.14 eV, and $\Delta E_{13} = E_{13} - E_{31}$ = 0.10 eV, where E_{ij} is the barrier height from state i to state j [Fig. 10(b)]. The above values will be justified by comparing the fitting curves with experimental data.

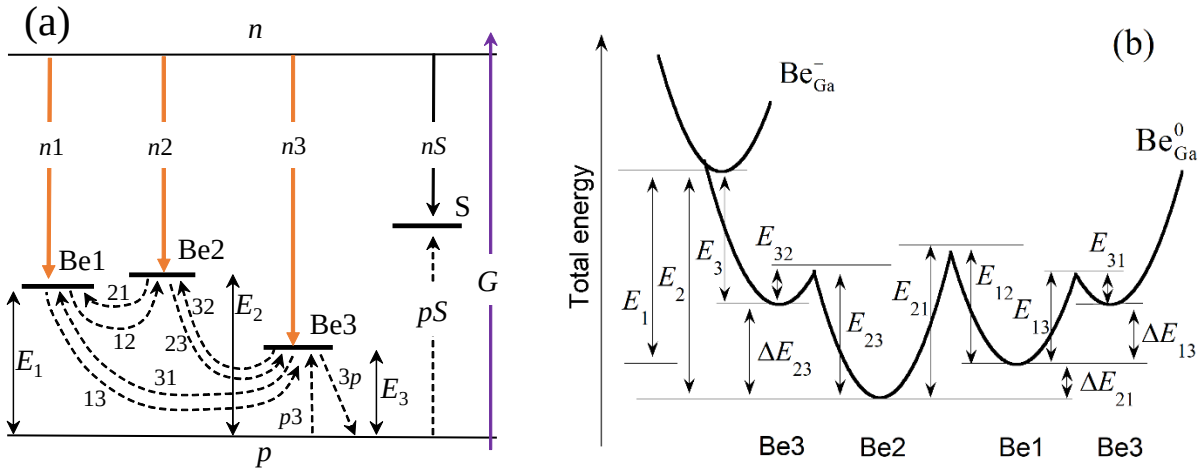

Fig. 10. Model of the Be_{Ga} acceptor in GaN. (a) Band diagram with three states of the Be_{Ga} acceptor (the –/0 transition levels) and a nonradiative defect S. Solid and dashed lines show transitions for electrons and holes, respectively. (b) Schematic adiabatic potentials for the Be_{Ga} acceptor: Be1 and Be2 are polaronic deep states, and Be3 is the shallow state.

The rate equations are written below according to charge flows shown in Fig. 10(a). The concentrations of the Be_{Ga} acceptors in states Be1, Be2, and Be3 are N_1^0, N_2^0, and N_3^0, respectively.

The concentrations of free holes and electrons are *p* and *n*. In steady-state conditions, the flows of holes via state Be3 can be described with the following equation:

$$\frac{dN_3^0}{dt} = \frac{p}{\tau_{p3}} + \frac{N_2^0}{\tau_{23}} + \frac{N_1^0}{\tau_{13}} - N_3^0\left(\frac{1}{\tau_{n3}} + \frac{1}{\tau_{32}} + \frac{1}{\tau_{31}} + \frac{1}{\tau_{3p}}\right) = 0. \quad (5)$$

For state Be2:

$$\frac{dN_2^0}{dt} = \frac{N_1^0}{\tau_{12}} + \frac{N_3^0}{\tau_{32}} - N_2^0\left(\frac{1}{\tau_{n2}} + \frac{1}{\tau_{21}} + \frac{1}{\tau_{23}}\right) = 0. \quad (6)$$

For state Be1:

$$\frac{dN_1^0}{dt} = \frac{N_3^0}{\tau_{31}} + \frac{N_2^0}{\tau_{21}} - N_1^0\left(\frac{1}{\tau_{n1}} + \frac{1}{\tau_{13}} + \frac{1}{\tau_{12}}\right) = 0. \quad (7)$$

Finally, for the nonradiative S center (assumed to be a deep donor for certainty):

$$\frac{dN_S^+}{dt} = \frac{p}{\tau_{pS}} - \frac{N_S^+}{\tau_{nS}} = 0. \quad (8)$$

The balance equation for holes in the valence band is:

$$\frac{dp}{dt} = G - p\left(\frac{1}{\tau_{p3}} + \frac{1}{\tau_{pS}}\right) + \frac{N_3^0}{\tau_{3p}} = 0. \quad (9)$$

That for electrons in the conduction band is:

$$\frac{dn}{dt} = G - \frac{N_1^0}{\tau_{n1}} - \frac{N_2^0}{\tau_{n2}} - \frac{N_3^0}{\tau_{n3}} - \frac{N_S^+}{\tau_{nS}} = 0. \quad (10)$$

In these equations, the characteristic times are $\tau_{p3} = \left(C_{p3}N_A^-\right)^{-1}$, $\tau_{pS} = \left(C_{pS}N_S^0\right)^{-1}$, $\tau_{3p} = \left(C_{p3}N_v\right)^{-1} g\exp\left(E_3/kT\right)$, $\tau_{ij} = \nu_{ij}^{-1}\exp\left(E_{ij}/kT\right)$, $\tau_{ni} = \left(C_{ni}n\right)^{-1}$, $\tau_{nS} = \left(C_{nS}n\right)^{-1}$, where i, j = 1, 2, 3. E_3 is the ionization energy for the Be3 state. ν_{ij} (all of the order of 10^{13} s^{-1}) are vibrational frequencies for transitions over potential barriers. $N_A = N_1^0 + N_2^0 + N_3^0 + N_A^-$ and $N_S = N_S^0 + N_S^+$.

For SI samples, one must also include shallow donors with the concentration N_D and charge conservation equations [20]. However, for conductive *n*-type GaN and low excitation intensities, we can assume $N_A^- = N_A$, $N_S^0 = N_S$, take n from the experiment, and solve the system of equations (5)-(9) analytically.

The solutions for the IQEs of PL via states Be1, Be2, and Be3 are

$$\eta_{Be1}^{YL} = \frac{\eta_0}{a_2\left(a_1 a_3 - \frac{\tau_{n2}}{\tau_{23}}\right) - \frac{\tau_{n1}}{\tau_{13}}} \tag{11}$$

$$\eta_{Be2}^{YL} = a_2 \eta_{Be1}^{YL} \tag{12}$$

$$\eta_{Be3}^{UVL} = a_1 \eta_{Be2}^{YL} \tag{13}$$

Here, $\eta_0 = \left(1+\tau_{p3}/\tau_{pS}\right)^{-1}$ is the IQE of the Be_{Ga}-related luminescence in the limit of low temperatures, and parameters a_1, a_2, and a_3 are

$$a_1 = \frac{\frac{\tau_{32}}{\tau_{n3}}\left[1+\frac{\tau_{n2}}{\tau_{23}}+\left(\frac{\tau_{12}}{\tau_{n1}}+\frac{\tau_{12}}{\tau_{13}}\right)\left(1+\frac{\tau_{n2}}{\tau_{21}}+\frac{\tau_{n2}}{\tau_{23}}\right)\right]}{\left(1+\frac{\tau_{12}}{\tau_{n1}}+\frac{\tau_{12}}{\tau_{13}}+\frac{\tau_{32}}{\tau_{31}}\right)}, \tag{14}$$

$$a_2 = \frac{\tau_{31}}{\tau_{32}}\frac{1+\frac{\tau_{n1}}{\tau_{13}}+\frac{\tau_{n1}}{\tau_{12}}\left(1+\frac{\tau_{32}}{\tau_{31}}\right)}{1+\frac{\tau_{n2}}{\tau_{23}}+\frac{\tau_{n2}}{\tau_{21}}\left(1+\frac{\tau_{31}}{\tau_{32}}\right)}, \tag{15}$$

$$a_3 = 1+\frac{\tau_{n3}}{\tau_{32}}+\frac{\tau_{n3}}{\tau_{31}}+\frac{\tau_{n3}\left(1-\eta_0\right)}{\tau_{3p}}. \tag{16}$$

It can be shown that at $T > 100$ K and for proposed parameters, the ratio between the UVL_{Be3} and YL_{Be2} intensities is

$$\frac{I_{Be3}^{UVL}}{I_{Be2}^{YL}} = a_1 \approx \delta \exp\left(-\frac{\Delta E_{23}}{kT}\right) \tag{17}$$

with $\delta = \tau_{n2} / \tau_{n3}$. Thus, the $I_{Be3}^{UVL} / I_{Be2}^{YL}$ ratio is a straight line with a slope $\Delta E_{23}/k$ in the Arrhenius plot. The ratio of the integrated intensities UVL_{Be3}/YL_{Be} for several GaN:Be samples is shown in Fig. 9. The fit using Eq. (17) with ΔE_{23} = 140 meV and δ = 18 is shown for sample 0020-1, for which the UVL_{Be3} band could be studied in the broadest temperature range. The parameter δ is slightly smaller or larger for other samples, but the ΔE_{23} (the slope) is the same. The variation in δ can be partly attributed to uncertainties in PL lifetimes since the PL decays are not strictly exponential, especially in SI samples.

Let us analyze the results of calculations for the Be_{Ga} defect with states Be1, Be2, and Be3. Photogenerated holes are captured by state Be3 (we ignore the capture of holes by the Be1 and B2 states and the emission of holes from these states to the valence band). The system almost immediately transfers from Be3 to Be1 over an insignificant barrier (E_{31} < 0.02 eV). Otherwise, the UVL_{Be3} band should be observed at T = 18 K. The experimental results can be well explained in two possible models. In Model A, barriers between Be1 and Be2 are high, and the barrier from Be3 to Be2 is relatively low ($E_{32} \approx 0.07$ eV). The magnitude of barrier E_{32} affects the characteristic temperature T_1, at which state Be2 becomes populated with holes from Be3. The barrier E_{12} is 0.20 eV or higher (it is only essential that ΔE_{21} = 0.04 eV). In Model B, barrier E_{32} is high (0.10 eV or larger value provided that ΔE_{23} = 0.14 eV). The magnitude of the barrier E_{12} (about 0.17 eV) determines the characteristic temperature T_1. In this case, the state Be2 is populated with holes only via state Be1 and not directly from Be3.

In Model A (high barriers between states Be1 and Be2), the critical temperature of the first step T_1 can be found from the following equation

$$\tau_{n1} \approx \frac{\tau_{13}}{\tau_{31}}\tau_{32} = \frac{\nu_{31}}{\nu_{13}\nu_{32}}\exp\left(\frac{\Delta E_{13} + E_{32}}{kT}\right). \quad (18)$$

It can be interpreted as the system transits from Be1 to Be2 via Be3, not directly. In Model B (high barriers between states Be2 and Be3), T_1 can be determined from

$$\tau_{n1} \approx \tau_{12} = \frac{1}{\nu_{12}}\exp\left(\frac{E_{12}}{kT}\right). \quad (19)$$

In this case, the system directly transfers from Be1 to Be2 at $T = T_1$. For τ_{n1} = 10-60 μs, $T_1 \approx 100$ K when $\Delta E_{13} + E_{32}$ (Model A) or E_{12} (Model B) is about 0.17 eV. Note that the characteristic time of the transfer in Model A is equal to the product of partial transfer times; i.e., $\tau_{1\to3\to2} = \tau_{13}\tau_{32} = \tau_{12}$.

V. DISCUSSION

A. Dual nature of the Be_{Ga} acceptor in GaN

The experimental data shown in Fig. 9 suggest that the UVL band emerging at $T > T_1$ is the UVL_{Be3} band caused by electron transitions from the conduction band to the shallow state of the Be_{Ga} acceptor. A single slope in the temperature dependence of the UVL_{Be3}/YL_{Be} ratio at $T < T_2$ and $T > T_2$ indicates that populations of states Be2 and Be3 with holes depend only on the relative positions of these states (ΔE_{23} = 0.14 eV), even when thermal emission of holes from one of the state (Be3) begins.

The high IQE of the recombination via states Be1 and Be2 is dictated by the fast capture of photogenerated holes by state Be3 and the high concentration of the Be_{Ga} acceptors. The first quenching step corresponds to the transition from Be1 to Be2 at $T \approx T_1$ with no change in their total IQE because the same hole-capture channel (via the Be3 state) feeds both Be1 and Be2 recombination channels.

1. Explanation of SSPL

The suggested rate equation model allows us to explain a large amount of experimental data. In particular, the fits of the temperature dependences of the YL_{Be} and UVL_{Be3} intensities with Eqs. (11)-(13) are shown in Fig. 11(a) for a conductive *n*-type GaN:Be sample grown by MBE. For selected parameters, there is no difference between Models A (solid lines) and B (dashed lines) except for the region at $T < 70$ K for the Be2 component of the YL_{Be} band. The fits with Model A for *n*-type GaN:Be sample grown by MOCVD are shown in Fig. 11(b). Note that the parameters of the Be_{Ga} acceptor for both samples are the same, but the PL lifetimes and IQE are different according to detailed SSPL and TRPL measurements.

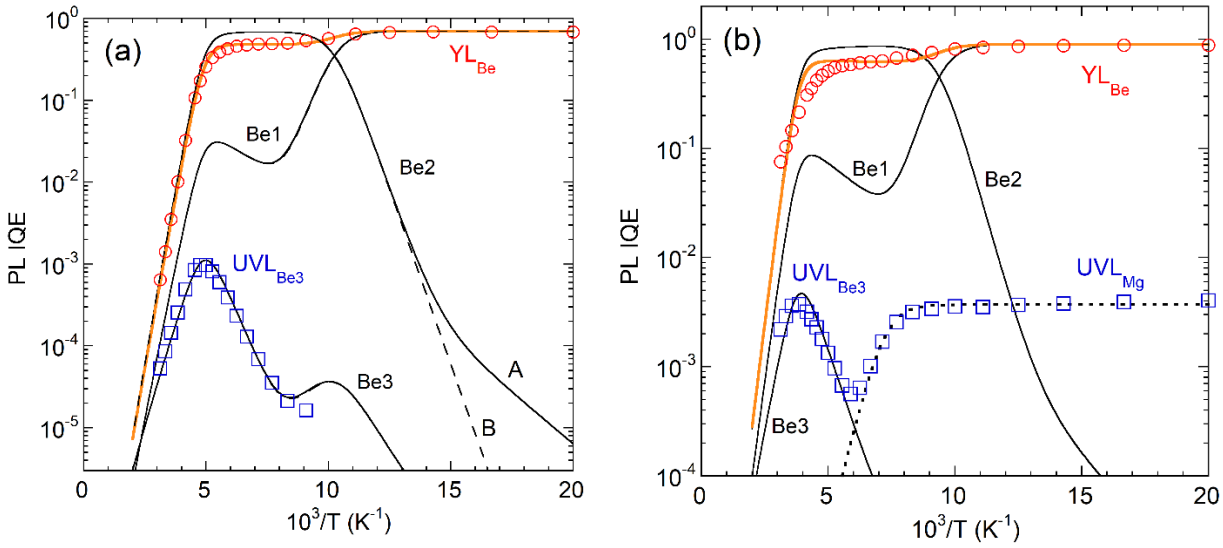

Fig. 11. Temperature dependences of PL IQE for the YL_{Be} and UVL_{Be3} bands. Symbols show experimental data. The lines Be1, Be2, and Be3 are calculated using Eq. (11)-(13) with the following parameters: E_{12} = 260 meV, E_{21} = 300 meV, E_{13} = 120 meV, E_{31} = 20 meV, E_{23} = 210 meV, E_{32} = 70 meV (Model A, solid lines), and E_{12} = 170 meV, E_{21} = 210 meV, E_{13} = 120 meV, E_{31} = 20 meV, E_{23} = 300 meV, E_{32} = 160 meV (Model B, dashed lines). $\nu_{ij} = 10^{13}$ s^{-1} for all i,j, γ = 0.3, and $C_{p3} = 4\times10^{-7}$ cm^3/s for both models. (a) MBE GaN:Be, sample 0020-1. τ_{n1} = 60 μs, τ_{n2} = 40 μs, τ_{n3} = 3.5 μs, η_0 = 0.7, and E_3 = 155 meV. (b) MOCVD GaN:Be, sample R26. τ_{n1} = 11 μs, τ_{n2} = 10 μs, τ_{n3} = 1.7 μs, η_0 = 0.9, and E_3 = 190 meV. The dotted line for the UVL_{Mg} band is calculated using Eq. (1) with the following parameters: $\eta_0(0) = 3.7\times10^{-3}$, $C_p = 1\times10^{-6}$ cm^3/s, τ_0 = 0.4 μs, and E_A = 165 meV.

It is essential to understand why the YL_{Be} band is quenched at $T > T_2$ with the activation energy of E_A = 0.30 eV. Previously, we attributed this quenching to the emission of holes from a level located at 0.3 eV above the VBM [12]. In the new model, we propose the thermal emission of holes from the shallow Be3 level located at 0.2 eV above the VBM. One may expect that the emission of holes from such a shallow level would cause PL quenching at much lower temperatures and with a smaller slope in the Arrhenius plot, similar to the quenching of the Mg-related UVL_{Mg} band [Fig. 11(b)]. However, analysis of the suggested model shows that the quenching of both the YL_{Be2} and UVL_{Be3} bands occurs at higher temperatures because the Be2 state feeds the Be3 state with holes. In particular, for conductive *n*-type GaN:Be, from Eqs. (5), (6), and (9), one can obtain an expression for the YL_{Be} quenching identical to Eq. (1) in which $\tau_0 = \tau_{n2}$, $C_p = C_{p3}$, and $E_A = E_3 + \Delta E_{23}$, where ΔE_{23} = 0.14 eV. The value of E_3 in the fits (0.155 eV in Fig. 11(a) and 0.19 eV in Fig. 11(b)) is smaller than the expected location of the UVL_{Be3} level above the VBM (0.21 eV at T = 190 K and 0.24 eV at T = 18 K). It is common that the ionization energies obtained from PL quenching (or from electrical measurements) are smaller than the energies E_i obtained from PL spectroscopy experiments, such as from observation of the ZPLs. In particular, the activation energy of the Mg-related UVL_{Mg} band is usually 0.15-0.19 eV (E_i = 0.223 eV at T = 18 K), and that of the Zn-related BL1 band is 0.30-0.35 eV (E_i = 0.40 eV at T = 18 K). There may be several reasons for this apparent disagreement [22].

The value of $C_{p3} = 4\times10^{-7}$ cm^3/s is found from the best fit of the thermal quenching of the YL_{Be} band. However, an acceptable agreement with the experiment can be achieved if parameters E_3 and C_{p3} are increased or decreased simultaneously within certain limits [29]. In particular, with $C_{p3} = 1\times10^{-6}$ cm^3/s and E_3 = 0.185 eV, the calculated curves in Fig. 11(a) still reasonably agree with the experimental data. Finally, from our experimental data, the possibility of insignificant

capture of holes by polaronic states and thermal emission of holes from these states to the valence band cannot be ruled out. The rates of these processes should be lower than those via the shallow Be_{Ga} state in proportion to the related hole-capture coefficients. We conclude that the C_p found earlier from the quenching of the YL_{Be} band (4×10^{-7} cm^3/s) is associated with the shallow Be_{Ga} state and is likely underestimated. The hole-capture coefficients for the deep polaronic states responsible for the YL_{Be} band are unknown.

2. Explanation of TRPL

Numerical calculations of differential equations (5)-(7) generally lead to the nonexponential decay of PL after pulse excitation. However, the decay can often be approximated with a single exponent where the effective PL lifetime is the time at which the $I^{PL}(t)t$ dependence has a maximum [24]. These effective PL lifetimes for the YL_{Be} and UVL_{Be3} bands and their temperature dependences agree with the ones found in the experiment with the same approach. In particular, assuming that $\tau_{n3} << \tau_{n2}$, we obtain from numerical solutions of differential equations (5)-(7) that the UVL_{Be3} band decays with the same PL lifetime as the YL_{Be2} band (τ_{n2}), and these PL lifetimes have the same temperature dependence.

3. Comparison with HSE calculations

Our preliminary calculations (300 atom hexagonal supercells, nudged elastic band method for potential barrier calculations) using HSE hybrid functional used in our previous work (α = 0.25, μ = 0.161 $Å^{-1}$) [5,30] qualitatively agree with the suggested model of the Be_{Ga} acceptor. These calculations predict three different configurations of the neutral Be_{Ga} acceptor shown in Fig. 12. The polaronic state with a hole localized on one of planar N neighbors (in-plane polaron) is the Be1 state [Fig. 12(a)]. The polaronic state with a hole localized on N neighbor along the wurtzite *c*-axis (axial polaron) is the Be2 state [Fig. 12(b)]. In both configurations, the hole is trapped by a

significant distortion of the Be-N bond, to 2.63 and 2.66 Å for Be1 and Be2 configurations, compared to 1.72 Å for the remaining Be-N bonds. From these HSE calculations the transition levels for the Be1 and Be2 configurations (0.57 and 0.58 eV for in-plane and axial polarons, respectively) and the expected PL band maxima (1.76 and 1.72 eV, respectively) are close, within the error of calculations. (see Ref. 5 for computational details). The small difference between the energies of the Be1 and Be2 configurations (0.01 eV in our calculations and 0.02 eV in Ref. 3) agrees with our experimental findings. The calculated Huang-Rhys factors for two polaronic bands are also very similar, 34 and 32 for Be1 and Be2, respectively. The delocalized state [Fig. 12(c)] corresponds to the model state Be3. In this case, the hole is weakly localized on multiple nitrogen neighbors of Be acceptor, with a lattice structure similar to that of bulk GaN, and the Be-N bonds decrease only slightly compared to bulk Ga-N bonds, by about 0.1 Å.

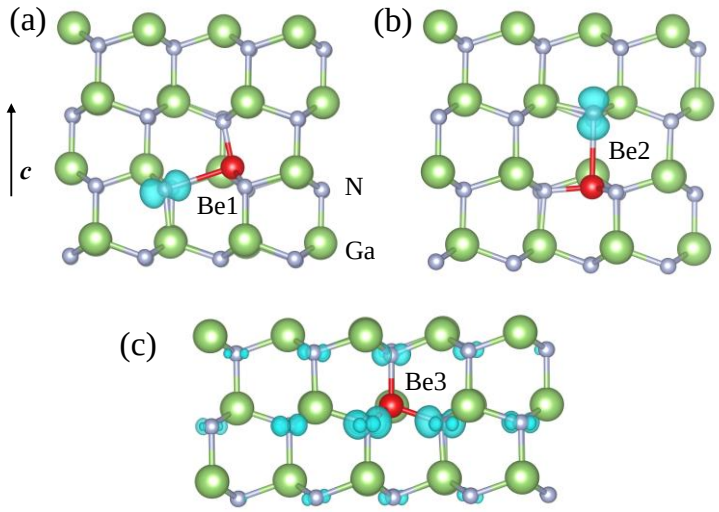

Fig. 12. HSE calculated spin density (isosurfaces at 10% of maximum values) of the neutral Be_{Ga} acceptor in two differently oriented deep polaronic states (a-b), and weakly localized shallow state (c). The arrow indicates the *c*-axis of wurtzite GaN. The Be_{Ga} acceptor configurations are labeled Be1-Be3 according to the model introduced in Sec. IV.

Figure 13 shows the calculated adiabatic potential landscape as a function of the absolute value of the configuration coordinate *Q*, as defined in Ref. 5, of the neutral Be_{Ga} acceptor in comparison with Models A and B that explain the experiment. (Strictly speaking, the directions of the *Q*-coordinate for transitions Be1 to Be2, Be2 to Be3, and Be1 to Be3 are not the same, as a one-dimensional picture might imply. However, this is insignificant for thermally activated processes discussed here.) The HSE calculations favor Model A (a relatively high barrier between configurations Be1 and Be2). However, our HSE calculations yield significantly deeper polaronic states (thermodynamic transition level is 0.58 eV from the VBM) than what follows from the experiment (0.33-0.38 eV). As a result, the barriers for transitions from deep states Be1 and Be2 to shallow state Be3 are much higher (Fig. 13).

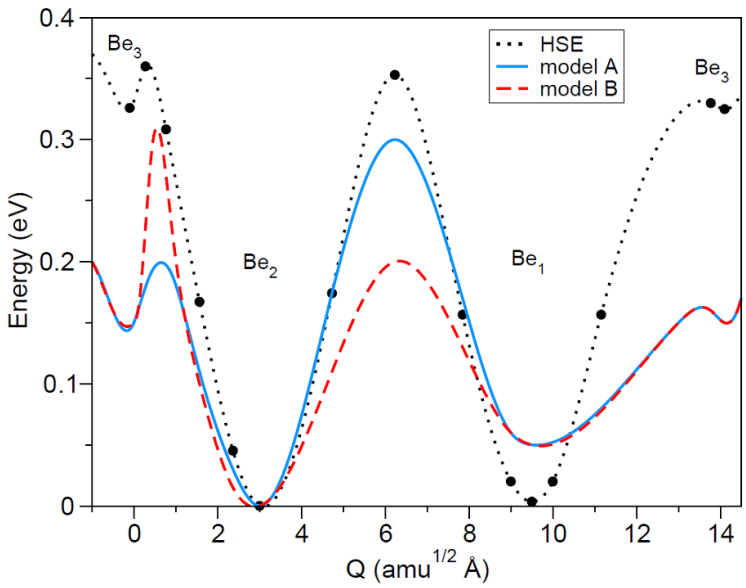

Fig. 13. Schematic one-dimensional potential landscape of the Be_{Ga} acceptor in the neutral state. Potential minima Be1 and Be2 correspond to two polaronic states, and Be3 is the shallow state. The solid blue and dashed red curves represent Models A and B, respectively, with the parameters given in the caption to Fig. 11. The dotted curve shows minima and barriers calculated using HSE hybrid functional.

4. On the origin of the UVL_{Be} band at 3.38 eV

We proposed earlier that the UVL_{Be} band with the first peak at 3.38 eV is caused by the shallow state of the Be_{Ga} acceptor located at 0.113 eV above the VBM. The YL_{Be} band was not associated with the deep state of the Be_{Ga} acceptor in that work because no correlation between the UVL_{Be} and YL_{Be} bands could be found [5,12]. Now, these attributions are revised. We conclude that the YL_{Be} band is caused by two polaronic states of the Be_{Ga} acceptor (Be1 and Be2). The shallow state of this acceptor is the Be3 state located at 0.24 eV above the VBM (in the limit of low temperatures). It contributes to PL spectra only at $T > 100$ K as the UVL_{Be3} band with a maximum at 3.26 eV. The question about the origin of the UVL_{Be} band at 3.38 eV remains unanswered, a challenge for future theoretical and experimental studies. What is known is that the related defect is the shallowest acceptor in GaN, which efficiently captures both electrons and holes (with $C_n \approx 10^{-11}$ cm^3/s and $C_p \approx 10^{-6}$ cm^3/s) [12,17]. It certainly contains Be, at least as a component. The defect can be passivated with hydrogen in GaN samples grown by MBE and MOCVD and requires annealing at $T \approx$ 750-900 °C for its activation. The results of the current work show that it is unlikely to be an isolated Be_{Ga} acceptor. It may be a Be-containing complex, the composition of which we could not find.

B. On the dual nature of other defects

1. Mg_{Ga} acceptor in GaN

The dual nature of acceptors was predicted also for other defects, including Mg_{Ga} acceptor in GaN and Li_{Zn} acceptor in ZnO [1]. In particular, Lany and Zunger [1] proposed that the UVL_{Mg} band in *n*-type GaN:Mg is caused by transitions via the shallow state of the Mg_{Ga}, while the broad blue band (BL_{Mg}) with a maximum at 2.7-2.9 eV in *p*-type samples is caused by transitions via its deep state. This explanation conflicts with the widely accepted attribution of the BL_{Mg} band to

electron transitions from deep donors to the shallow Mg_{Ga} acceptor [25,27,31,32]. Moreover, as we established for the Be_{Ga} acceptor in this work, a correlation between PL signals from deep and shallow states should be the same in all samples, independent of their conductivity type and the concentration of free charge carriers (see Fig. 9). However, in *n*-type GaN:Mg no contribution of the predicted blue band could be found in a wide temperature range [27]. Indeed, from analysis of the PL spectra, it follows that the integrated intensity from the predicted blue band (if this deep state exists) is lower, at least by a factor of 10-100, than that of the UVL_{Mg} band at temperatures between 18 and 100 K (Fig. 14).

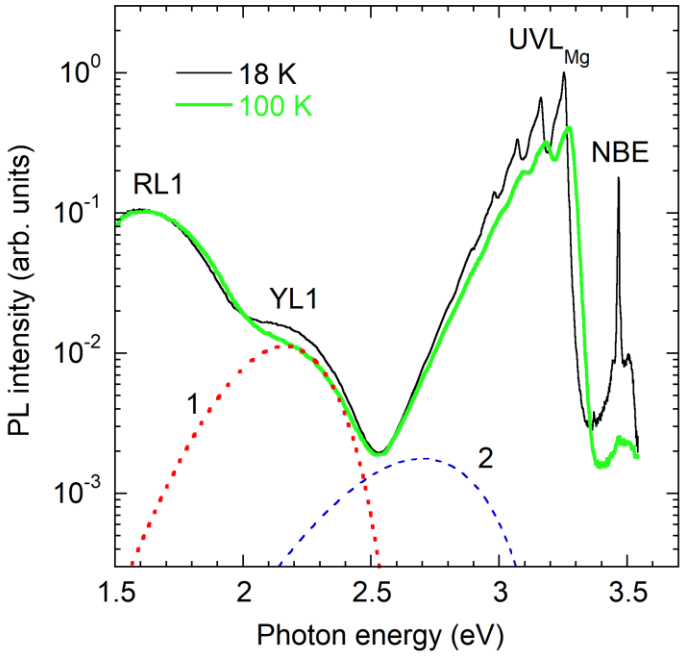

Fig. 14. PL spectra from Mg-doped *n*-type GaN (sample 3590) grown by HVPE on sapphire. The dashed curves are calculated shapes using a one-dimensional configuration coordinate model [33] for the C_N-related YL1 band (1) and predicted deep state of the Mg_{Ga} acceptor (2). Curve 2 has a maximum at 2.7 eV, according to [3]. The integrated PL intensity of curve 2 is 100 times lower than that of the UVL_{Mg} band. The PL lifetime of the UVL_{Mg} band is $\tau = 20$ μs for the UVL_{Mg} band at $T = 100$ K.

From experimental studies, the existence of two Mg-related acceptors (A1 and A2) in GaN was suggested by Monemar et al. [34]. In lightly doped GaN:Mg, the UVL_{Mg} band with the ZPL at 3.27 eV was observed along with the acceptor-bound-exciton (ABE) line at 3.466 eV. These features were attributed to an acceptor complex containing Mg and likely hydrogen (the A1 acceptor). In heavily doped GaN:Mg and especially after thermal annealing, a broad and weak PL band with a maximum at about 3.15 eV appeared, along with the ABE peak at 3.454 eV. These features were initially attributed to the isolated Mg_{Ga} acceptor (A2). However, later these researchers revised the above assignments [35]. The UVL_{Mg} band and the ABE peak at 3.466 eV were attributed to the isolated Mg_{Ga} acceptor, while the band at 3.15 eV and the ABE peak at 3.454 eV were associated with Mg atoms at stacking faults.

Thus, PL experiments show no reliable evidence for the deep polaronic state of the Mg_{Ga} acceptor in GaN. We may speculate that it is either unstable or causes very weak PL. It will be shown below that specific barriers between the shallow and deep states can explain why PL from only the shallow Mg_{Ga} state is observed.

From Eq. (6), modified to keep only two states – shallow and deep, the ratio of related PL intensities can be found as

$$\frac{I^{SS}}{I^{DS}} = \frac{\tau_{SS\to DS}}{\tau_{n\to SS}}\left(1+\frac{\tau_{n\to DS}}{\tau_{DS\to SS}}\right) = \frac{1+\tau_{n\to DS}\nu_{DS\to SS}\exp\left(\frac{-E_{DS\to SS}}{kT}\right)}{\tau_{n\to SS}\nu_{SS\to DS}\exp\left(\frac{-E_{SS\to DS}}{kT}\right)}, \tag{20}$$

where *n*, *SS*, and *DS* indicate the conduction band, shallow and deep states, respectively. The temperature dependence includes two regions, low- and high-temperature, that are approximated, respectively, with the following expressions:

$$\left(\frac{I^{SS}}{I^{DS}}\right)_{low-T} = \frac{\tau_{SS\to DS}}{\tau_{n\to SS}} = \frac{1}{\tau_{n\to SS}\nu_{SS\to DS}\exp\left(\frac{-E_{SS\to DS}}{kT}\right)} \quad (21)$$

$$\left(\frac{I^{SS}}{I^{DS}}\right)_{high-T} = \frac{\tau_{n\to DS}\nu_{DS\to SS}}{\tau_{n\to SS}\nu_{SS\to DS}}\exp\left(\frac{-\Delta E_{DS,SS}}{kT}\right) \quad (22)$$

Lany and Zunger [1] calculated that the difference between the shallow and deep states of the Mg_{Ga} acceptor in GaN is $\Delta E_{SS,DS}$ = 30 meV, and the barrier for the transition from the shallow to the deep state is about $E_{SS\to DS}$ = 20 meV. They suggested that only the UVL_{Mg} band from the Mg_{Ga} shallow state is observed in *n*-type GaN because the PL lifetime ($\tau_{n\to SS}$) is much shorter than the time of transfer to the deep state ($\tau_{SS\to DS}$), see Eq. (21).

Figure 15 shows the temperature dependence of the I^{SS}/I^{DS} ratio calculated using Eq. (20) with $\Delta E_{SS,DS}$ = 30 meV, $E_{SS\to DS}$ = 20 meV [1], $\tau_{n\to SS}$ = 10^{-5} s, and $\tau_{n\to DS}$ = 10^{-3} s (the solid green curve). The decreasing with temperature ratio corresponds to thermally activated transitions of holes from the shallow state to the deep state over the barrier $E_{SS\to DS}$ and can be fitted with Eq. (21). The increasing with temperature ratio (described with Eq. (22)) corresponds to thermally activated transitions of holes from the deep state to the shallow state, similar to the processes depicted in Fig. 9 for the Be_{Ga} acceptor. We can see that for the chosen parameters, the PL from the shallow Mg_{Ga} state (the UVL_{Mg} band) should be weaker than the blue PL band from the deep state at temperatures between 18 and 100 K, which contradicts experiments for *n*-type GaN where the deep state of the Mg_{Ga} could not be found ($I^{SS}/I^{DS} > 100$) between 18 and 100 K (Fig. 14) [27]. To resolve the contradiction, the parameters must be modified. An example is shown with the orange line for which $\tau_{n\to DS}/\tau_{n\to SS} = 1000$, $\Delta E_{SS,DS}$ = 10 meV, and $E_{SS\to DS}$ = 100 meV. Note that

the $\tau_{n\to DS}/\tau_{n\to SS}$ ratio is equal to the ratio of electron-capture coefficients C_n^{SS}/C_n^{DS} in *n*-type GaN, and the latter is unlikely to exceed 10^3 [6,25].

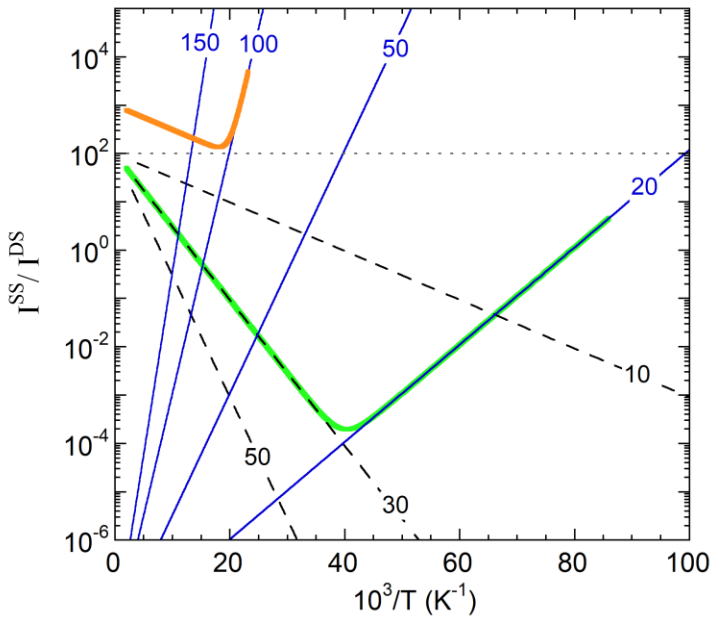

Fig. 15. Temperature dependence of the I^{SS}/I^{DS} ratio calculated using Eqs. (20)-(22). The solid blue lines are calculated using Eq. (21) with $\tau_{n\to SS}$ = 0.01 ms and $E_{SS\to DS}$ = 20, 50, 100, and 150 meV. The dashed lines are calculated using Eq. (22) with $\tau_{n\to SS}/\tau_{n\to DS}$ = 100 and $\Delta E_{DS,SS}$ = 10, 30, and 50 meV. The solid green line is calculated using Eq. (20) with $\tau_{n\to SS}$ = 0.01 ms, $\tau_{n\to DS}$ = 1 ms, $E_{SS\to DS}$ = 20 meV and $\Delta E_{DS,SS}$ = 30 meV. The solid orange line is calculated using Eq. (20) with $\tau_{n\to SS}$ = 0.01 ms, $\tau_{n\to DS}$ = 10 ms, $E_{SS\to DS}$ = 10 meV, and $\Delta E_{DS,SS}$ = 100 meV. ν_{ij} = 10^{13} s^{-1} in all the cases. In the experiment, I^{SS}/I^{DS} > 100 in the whole temperature range, and the boundary for this condition is indicated with the horizontal dotted line.

We conclude that the barrier between the two configurations must be at least 100 meV, and the deep state (if it exists) must be deeper than the shallow state by less than ~10 meV. Then, only the UVL_{Mg} band will be observed in a wide range of temperatures in *n*-type GaN. Note that if the PL band from the deep state has a maximum at higher photon energies (the theoretical predictions may not be accurate), the restrictions for the barrier between the two states are softened. For

example, if $\hbar\omega_{max}$ = 3.1 eV, the deep state-related structureless PL band would be hidden under the UVL_{Mg} band and may not be resolved with increasing temperature if the barrier between the two configurations is ~50 meV.

2. *Li_{Zn} acceptor in ZnO*

The Li_{Zn} acceptor in ZnO with the –/0 level at 0.65±0.10 eV above the VBM is responsible for the orange luminescence (OL or OL_{Li}) band with a maximum at 2.0 eV [36-39]. Two deep polaronic states of the Li_{Zn} acceptor were studied by electron paramagnetic resonance (EPR) and luminescence [37,38]. In particular, Meyer et al. [38] have found that the "axial" configuration (a hole trapped at an oxygen ion located along the c-axis of the crystal in the neighborhood of the Li_{Zn} defect) has a minimum 34 meV deeper than that of "non-axial" centers (a hole trapped at one of three non-axially bound oxygen atoms). The population of the axial and non-axial centers with holes can be varied by temperature and quantified by the strength of the EPR signals [38] or luminescence polarization [37]. Meyer et al. [40] also observed in some ZnO:Li samples at T = 4.2 K a UVL band with the strongest peak at 3.05 eV followed by LO phonon replicas. The binding energy of the related acceptor was estimated to be 300 meV. Since this UVL band completely disappeared after rapid thermal annealing at 820 °C for 5 s, it was attributed to a hydrogen-containing complex such as Li_{Zn}-H-Li_{Zn} [40].

Lany and Zunger [1] predicted the dual nature of the Li_{Zn} acceptor and calculated that the difference between the deep and shallow states is 0.43 eV. These authors proposed that the OL_{Li} band (2.0 eV) and the UVL_{Li} band (3.05 eV) in Li-doped ZnO are associated with the deep and shallow states of the Li_{Zn} acceptor. Based on the results for the Be_{Ga} in GaN, we expect a correlation between PL from shallow and deep states, identical in all samples. However, at least in some ZnO samples, the integrated PL intensity of the OL_{Li} band is 10^2-10^3 times higher than a

possible contribution of the shallow state (at 3.05 eV) between 10 and 250 K [39,41]. Our calculations with Eq. (20) and $\Delta E_{DS,SS}$ = 430 meV indicate that the UVL band would not be observed in this temperature range if the shallow to deep state barrier is lower than 20 meV (Figs. 15 and 16). Otherwise, the UVL_{Li} band (the shallow state) must be stronger than the OL_{Li} band (the deep state) in all ZnO:Li samples, at least at T < 20 K, which contradicts experiments [39,41]. Unlike the UVL_{Be3} band in GaN:Be ($\Delta E_{DS,SS}$ = 0.14 eV), the UVL_{Li} band in ZnO will not emerge with increasing temperature provided that $\Delta E_{DS,SS}$ > 0.4 eV.

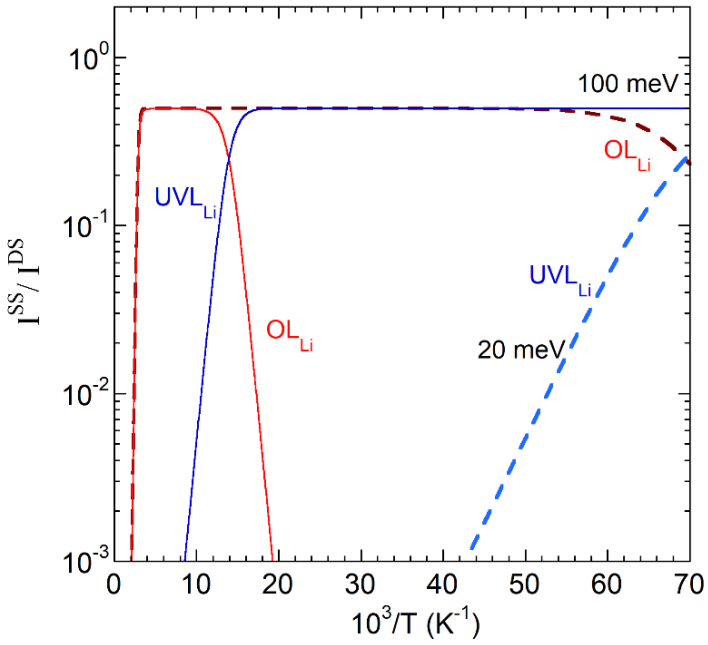

Fig. 16. Temperature dependence of PL intensities of the OL_{Li} band (the deep state of the Li_{Zn}) and the UVL_{Li} band (the shallow state of the Li_{Zn}) calculated with Eq. (20). $E_{SS\rightarrow DS}$ = 100 meV (the solid lines) and $E_{SS\rightarrow DS}$ = 20 meV (the dashed lines). $\Delta E_{DS,SS}$ = 430 meV, τ_{SS} = 1 μs, τ_{DS} = 100 μs, $\nu_{ij} = 10^{13}$ s^{-1} for all the curves.

Thus, experiments do not confirm so far the predicted dual nature for acceptors such as Mg_{Ga} in GaN and Li_{Zn} in ZnO. To the best of our knowledge, the Be_{Ga} acceptor in GaN is the first reliable

experimental confirmation of this prediction. In light of these new findings, we revise our previous conclusions presented in Ref. 5. For dual nature defects in semiconductors, deep polaronic states are observable in PL experiments, even if the carrier capture rates for these states are significantly lower than those for the accompanying delocalized states. According to the above analysis, potential barriers between these states may be crucial for observing PL from the deep or shallow state.

VI. CONCLUSION

The theoretically predicted dual nature of acceptors in semiconductors is confirmed by PL experiments with an example of the Be_{Ga} defect in GaN. The defect has three states: two deep (polaronic) states with the –/0 transition levels at 0.3-0.4 eV above the VBM and a shallow state (delocalized hole) at 0.2 eV above the VBM. Only one of these states (the shallow state Be3) efficiently captures holes from the valence band and emits them back at $T > 200$ K. We do not find experimental evidence for the dual nature of other defects, such as Mg_{Ga} in GaN and Li_{Zn} in ZnO. The rate equation model indicates that the observation of both states (shallow and deep) in PL experiments may be hampered by too high or too low potential barriers between the defect configurations.

ACKNOWLEDGMENTS

The work at VCU and SUNY was supported by the National Science Foundation under grants DMR-1904861 and DMR-1905186, respectively.

The authors have no conflicts of interest.

References

[1] S. Lany and A. Zunger, "Dual nature of acceptors in GaN and ZnO: The curious case of the shallow Mg_{Ga} deep state", Appl. Phys. Lett. **96**, 142114 (2010).

[2] S. Lany, "Predicting polaronic defect states by means of generalized Koopmans density functional calculations", Phys. Stat. Sol. (b) **248**, 1052-1060 (2011).

[3] J. L. Lyons, A. Janotti, and C. G. Van de Walle, "Impact of group-II acceptors on the electrical and optical properties of GaN", Jap. J. Appl. Phys. **52**, 08JJ04 (2013).

[4] X. Cai, J. Yang, P. Zhang, and S.-H. Wei, "Origin of Deep Be Acceptor Levels in Nitride Semiconductors: The Roles of Chemical and Strain Effects", Phys. Rev. Appl. **11**, 034019 (2019).

[5] D. O. Demchenko, M. Vorobiov, O. Andrieiev, T. H. Myers, and M. A. Reshchikov, "Shallow and deep states of beryllium acceptor in GaN: Why photoluminescence experiments do not reveal small polarons for defects in semiconductors", Phys. Rev. Lett. **126**, 027401 (2021).

[6] M. A. Reshchikov, "Measurement and analysis of photoluminescence in GaN", J. Appl. Phys. **129**, 121101 (2021).

[7] F. J. Sánchez, F. Calle, M. A. Sánchez-García, E. Calleja, E. Muñoz, C. H. Molloy, D. J. Somerford, J. J. Serrano, and J. M. Blanco, "Experimental evidence for a Be shallow acceptor in GaN grown on Si(111) by molecular beam epitaxy", Semicond. Sci. Technol. **13**, 1130-1133 (1998).

[8] H. Teisseyre, I. Gorczyca, N. E. Christensen, A. Svane, F. B. Naranjo, and E. Calleja, "Pressure behavior of beryllium-acceptor level in gallium nitride", J. Appl. Phys. **97**, 043704 (2005).

[9] D. J. Dewsnip, A. V. Andrianov, I. Harrison, J. W. Orton, D. E. Lacklison, G. B. Ren, S. E. Hooper, T. S. Cheng, and C. T. Foxon, "Photoluminescence of MBE grown wurtzite Be-doped GaN", Semicond. Sci. Technol. **13**, 500-504 (1998).

[10] M. Jaworek, A. Wysmolek, M. Kaminska, A. Twardowski, M. Bockowski, and I. Grzegory, "Photoluminescence Study of Bulk GaN Doped with Beryllium", Acta Physica Polonica A **108**, 705-710 (2005).

[11] H. Teisseyre, J. L. Lyons, A. Kaminska, D. Jankowski, D. Jarosz, M. Bockowski, A. Suchocki, and C. G. Van de Walle, "Identification of yellow luminescence centers in Be-doped GaN through pressure-dependent studies", J. Phys. D: Appl. Phys. **50**, 22LT03 (2017).

[12] M. Vorobiov, O. Andrieiev, D. O. Demchenko, and M. A. Reshchikov, "Point Defects in Beryllium Doped GaN", Phys. Rev B **104**, 245203 (2021).

[13] F. B. Naranjo, M. A. Sánchez-García, J. L. Pau, A. Jiménez, E. Calleja, E. Muñoz, J. Oila, K. Saarinen, and P. Hautojärvi, "Study of the Effects of Mg and Be Co-doping in GaN Layers", Phys. Stat. Sol. (a) **180**, 97-102 (2000).

[14] M. A. Reshchikov, O. Andrieiev, M. Vorobiov, D. Ye, D. O. Demchenko, K. Sierakowski, M. Bockowski, B. McEwen, V. Meyers, and F. Shahedipour-Sandvik, "Thermal annealing of GaN implanted with Be", J. Appl. Phys. **131**, 125704 (2022).

[15] M. A. Reshchikov, O. Andrieiev, M. Vorobiov, D. O. Demchenko, B. McEwen, and F. Shahedipour-Sandvik, "Photoluminescence from GaN implanted with Be and F", Phys. Stat. Sol. (b) 2300131 (2023).

[16] B. McEwen, M. A. Reshchikov, E. Rocco, V. Meyers, K. Hogan, O. Andrieiev, M. Vorobiov, D. O. Demchenko, and F. Shahedipour-Sandvik, "MOCVD Growth and Characterization of Be-Doped GaN", ACS Applied Electronic Materials **4**, 3780-3785 (2022).

[17] M. A. Reshchikov, M. Vorobiov, O. Andrieiev, B. McEwen, E. Rocco, V. Meyers, D. O. Demchenko, and F. Shahedipour-Sandvik, "Photoluminescence from Be-Doped GaN Grown by Metal-Organic Chemical Vapor Deposition", Phys. Stat. Sol. (b) 202200487 (2022).

[18] K. Lee, "Issues for p-type doping of gallium nitride with beryllium and magnesium grown by rf-plasma assisted molecular beam epitaxy", Ph.D., West Virginia University, United States – West Virginia (2007).

[19] M. A. Reshchikov, M. A. Foussekis, J. D. McNamara, A. Behrends, A. Bakin, and A.Waag, "Determination of the absolute internal quantum efficiency of photoluminescence in GaN co-doped with Zn and Si", J. Appl. Ph*ys*. **111**, 073106 (2012).

[20] M. A. Reshchikov, A. A. Kvasov, M. F. Bishop, T. McMullen, A. Usikov, V. Soukhoveev, and V. A. Dmitriev, "Tunable and abrupt thermal quenching of photoluminescence in high-resistivity Zn-doped GaN", Phys. Rev. B **84**, 075212 (2011).

[21] M. A. Reshchikov, M. Vorobiov, D. O. Demchenko, Ü. Özgür, H. Morkoç, A. Lesnik, M. P. Hoffmann, F. Hörich, A. Dadgar, and A. Strittmatter, "Two charge states of the C_N acceptor in GaN: Evidence from photoluminescence", Phys. Rev. B **98**, 125207 (2018).

[22] M. A. Reshchikov, "Mechanisms of thermal quenching of defect-related luminescence in semiconductors", Phys. Stat. Sol. (a) **218**, 2000101 (2020).

[23] M. A. Reshchikov, "Time-resolved photoluminescence from defects in GaN", J. Appl. Phys. **115**, 103503 (2014).

[24] R. Y. Korotkov, M. A. Reshchikov, and B. W. Wessels, "Acceptors in undoped GaN studied by transient photoluminescence", Physica B **325**, 1-7 (2003).

[25] M. A. Reshchikov and H. Morkoç, "Luminescence properties of defects in GaN", J. Appl. Phys. **97**, 061301 (2005).

[26] M. A. Reshchikov, J. D. McNamara, M. Toporkov, V. Avrutin, H. Morkoç, A. Usikov, H. Helava, and Yu. Makarov, "Determination of the electron-capture coefficients and the concentration of free electrons in GaN from photoluminescence", Scientific Reports **6**, 37511 (2016).

[27] M. A. Reshchikov, P. Ghimire, and D. O. Demchenko, "Magnesium acceptor in gallium nitride: I. Photoluminescence from Mg-doped GaN", Phys. Rev. B **97**, 205204 (2018).

[28] B. Monemar, "Fundamental energy gap of GaN from photoluminescence excitation spectra", Phys. Rev. B **10**, 676-681 (1974).

[29] M. A. Reshchikov, "Photoluminescence from defects in GaN", Proceedings of SPIE-The International Society for Optical Engineering, Gallium Nitride Materials and Devices XVIII,

ed. H. Fujioka, H. Morkoç, and U. Schwarz, **12421**, 1242109 (2023). Doi: 10.1117/12.2645878

[30] D. O. Demchenko and M. A. Reshchikov, "Hydrogen passivation of the beryllium acceptor in GaN and a possible route for *p*-type doping", Appl. Phys. Lett. **118**, 142103 (2021).

[31] L. Eckey, V. von Gfug, J. Holst, A. Hoffmann, A. Kaschner, H. Siegle, C. Thomsen, B. Schineller, K. Heime, M. Heuken, O. Schön, and R. Beccard, "Photoluminescence and Raman study of compensation effects in Mg-doped GaN epilayers", J. Appl. Phys. **84**, 5828-5830 (1998).

[32] U. Kaufmann, M. Kunzer, H. Obloh, M. Maier, Ch. Manz, A. Ramakrishnan, and B. Santic, "Origin of defect-related photoluminescence bands in doped and nominally undoped GaN", Phys. Rev. B **59**, 5561-5567 (1999).

[33] M. A. Reshchikov, D. O. Demchenko, J. D. McNamara, S. Fernández-Garrido, and R. Calarco, "Green luminescence in Mg-doped GaN", Phys. Rev. B **90**, 035207 (2014).

[34] B. Monemar, P. P. Paskov, G. Pozina, C. Hemmingsson, J. P. Bergman, T. Kawashima. H. Amano, I. Akasaki, T. Paskova, S. Figge, D. Hommel, and A. Usui, "Evidence for Two Mg Related Acceptors in GaN", Phys. Rev. Lett. **102**, 235501 (2009).

[35] B. Monemar, S Khromov, G. Pozina, P. Paskov, P. Bergman, C. Hemmingsson, L. Hultman, H. Amano, V. Avrutin, X. Li, and H. Morkoç, "Luminescence of Acceptors in Mg-Doped GaN", Jap. J. Appl. Phys. **52**, 08JJ03 (2013).

[36] D. Zwingel, "Trapping and recombination processes in the thermoluminesce of Li-doped ZnO single crystals", J. Lumin. **5**, 385-405 (1972).

[37] O. F. Schirmer and D. Zwingel, "The yellow luminescence of zinc oxide", Sol. St. Comm. **8**, 1559-1563 (1970).

[38] B. K. Meyer, A. Hofstaetter, and V. V. Laguta, "Tunneling phenomena of trapped holes in ZnO:Li", Physica B **376-377**, 682-685 (2006).

[39] J. D. McNamara, N. M. Albarakati, and M. A. Reshchikov, "Abrupt and tunable quenching of photoluminescence in ZnO", J. Lumin. **178**, 301-306 (2016).

[40] B. K. Meyer, J. Stehr, A. Hofstaetter, N. Volbers, A. Zeuner, and J. Sann, “On the role of group I elements in ZnO”, Appl. Phys. A **88**, 119-123 (2007).

[41] M. A. Reshchikov, B. Nemeth, J. Nause, J. Xie, B. Hertog, A. Osinsky, V. Avrutin, N. Izyumskaya, R. Shimada, and H. Morkoç, “Visible Luminescence Related to Defects in ZnO”, MRS Online Proceedings Library **1035**, 305 (2007). https://doi.org/10.1557/PROC-1035-L03-05